Dynamic reorganization and selective segregation of mitochondria under DarT-mediated mtDNA damage

Nitish Dua, Akshaya Seshadri and Anjana Badrinarayanan*

National Centre for Biological Sciences - Tata Institute of Fundamental Research, Bellary Road, Bangalore 560065, Karnataka, India, Phone: 91 80 23666547

*Correspondence to: anjana@ncbs.res.in

Keywords

S. cerevisiae, mtDNA, DNA damage, mitochondrial fission and fusion, DarT, single-cell imaging, fluorescence microscopy

Abstract:

Mitochondria are dynamic organelles that play essential roles in cell growth and survival. Two key processes of fission and fusion are critical for the distribution, segregation and maintenance of mitochondria and their genomes (mtDNA). While recent work has begun to elucidate the importance of mitochondrial organization for mitochondrial genome maintenance, the impact of mtDNA perturbations on mitochondrial dynamics and/ or organellar maintenance remains less understood. To address this, we develop a tool to induce mitochondria-specific DNA damage, using a mitochondrial-targeted base modifying bacterial toxin, DarT. Following damage induction, we observe dynamic reorganization of the mitochondrial network. We find that mtDNA damage predominantly affects rates of fusion, likely driven by mitochondrial dysfunction arising due to DNA damage. Changes in network organization are associated with loss of mtDNA, independent of mitophagy. Unexpectedly, we find that perturbation to exonuclease function of the mtDNA replicative polymerase, Mip1, results in rapid loss of mtDNA. Our data suggest that, under damage, the partitioning of defective mtDNA and organelle can be de-coupled, with an emphasis on mitochondrial segregation even in the absence of its DNA. Together, our works reveals the importance of genome maintenance on mitochondrial function, that can act as a modulator of organelle organization and segregation.

45 **Introduction:**

46 Mitochondrial networks are highly dynamic and undergo changes in shape and size
47 throughout the cell cycle (Westermann, 2010). These dynamics are predominantly attributed
48 to two processes of fission and fusion, carried out by evolutionarily conserved machineries
49 (Westermann, 2008). In budding yeast, fission of mitochondria is carried out by DNM1, which
50 is recruited to the outer membrane by adaptor proteins. Fusion of mitochondria occurs at the
51 level of the inner membrane (carried out by Mgm1) as well as the outer membrane, via Fzo1
52 (Scott & Youle, 2010; Shaw & Nunnari, 2002). Fission and fusion are required for its proper
53 distribution and segregation during cell division and also essential for moulding the organelle
54 network in response to changing growth conditions (Detmer & Chan, 2007). Along with
55 facilitating dynamic adaptation of mitochondrial function to the metabolic needs of the cell
56 (Bagamery et al., 2020; Laporte et al., 2018), they play a crucial role in quality control of the
57 organelle (Detmer & Chan, 2007; Ni et al., 2015).

58 Apart from ensuring organelle health, fission and fusion are also important for maintaining
59 mitochondrial genome integrity and its DNA copy numbers (Busch et al., 2014; Lewis et al.,
60 2016; Lieber et al., 2019; Osman et al., 2015). All eukaryotic cells, with a few exceptions,
61 contain multiple copies of mtDNA (chiefly encoding for part of the electron transport chain
62 as well as mitochondrial translation proteins) and are distributed throughout the organelle
63 network (Brown et al., 2011; Chen & Butow, 2005; Osman et al., 2015). These DNA copies are
64 packaged in the form of nucleoids (Farge et al., 2012), primarily by Abf2 in budding yeast
65 (Chen & Butow, 2005). Studies have shown that mtDNA nucleoids are non-randomly
66 distributed in the mitochondrial network, and are present equidistant from each other
67 (Osman et al., 2015). This organization appears to be essential for ensuring segregation of
68 accurate amounts of mtDNA during cell division (Jajoo et al., 2016). Indeed, lowered levels of
69 mtDNA replication are observed when mitochondrial fusion is perturbed, leading to a
70 decrease in mtDNA copy numbers (Ramos et al., 2019). Mitochondrial fission is also linked to
71 mtDNA replication and segregation in budding yeast and facilitates distribution of mtDNA
72 throughout the mitochondrial network (Lewis et al., 2016). Previous studies have also
73 reported that deletions on mtDNA occur when pathways of fission and fusion are perturbed
74 (Osman et al., 2015).

75 Accurate maintenance of mtDNA integrity is critical, as mutations on mtDNA can have adverse
76 effects on cell survival and are associated with several human pathologies (Hahn & Zuryn,

2019; Scheibye-Knudsen et al., 2015; Taylor & Turnbull, 2005). Close proximity of mtDNA to the electron transport chain makes it susceptible to damage via reactive species generated during oxidative phosphorylation (Alexeyev et al., 2013; Yakes & Van Houten, 1997). Even under physiological conditions, mtDNA accumulates mutations and deletions over time; these are also proposed to be major drivers of ageing (Alexeyev et al., 2013; Richter, 1995; Wallace, 2010).

How do cells respond to mtDNA damage? There is evidence for the localization of certain DNA repair proteins to the mitochondria (such as those involved in base excision repair and recombination) (Alexeyev et al., 2013; Boesch et al., 2011; Scheibye-Knudsen et al., 2015; Stevnsner et al., 2002). However, certain repair pathways seem to be absent from the mitochondria (for example, nucleotide excision repair) (Clayton et al., 1974; Pascucci et al., 1997). Thus, while DNA repair pathways have been detected in the mitochondria, importance and regulation of mtDNA damage repair has remained unclear. Since mtDNA can directly affect functionality of the organelle, it is possible that one layer of quality control is carried out by mechanisms that respond to mitochondrial dysfunction directly. Indeed, in response to organelle dysfunction, cells employ fission and fusion machineries to clear out any damaged mitochondria (Ni et al., 2015). For example, regulation of fusion can facilitate complementation of mutations present on mitochondrial genomes (Nakada et al., 2001). Similarly, mitochondrial fission helps in selective removal and degradation of mitochondria via PINK-Parkin mediated mitophagy or even mitocytosis (Jiao et al., 2021; Jin & Youle, 2012; Zhang et al., 2019). More recently, a role for mitochondrial reorganization at the level of the cristae has also been discovered to contribute to segregation of defective mitochondrial domains, arising from mutant mtDNA copies (Jakubke et al., 2021). It is likely that these pathways contribute to different degrees of quality control, depending on the cell type and specific growth environments (Pickles et al., 2018). Although it is becoming increasingly evident that mitochondrial dynamics can regulate mtDNA synthesis, partitioning and homeostasis, the influence of mtDNA damage on mitochondrial organization and segregation is not fully understood. A major challenge in studying mtDNA damage response and repair has been the ability to generate mtDNA-specific damage. In this context, tools to make mtDNA-specific DSBs have been invaluable, but are dependent on the presence of specific sequences on the mtDNA to allow for targeted action of the enzyme. In most cases, generic

damaging agents that can cause adducts or lesions on DNA preclude the ability to disentangle mitochondria-specific effects.

To characterize the impact of mtDNA perturbations on organelle organization and function, we developed a novel system to generate inducible mtDNA-specific damage in *S. cerevisiae*. We engineered a mitochondrially-targeted bacterial toxin, mtDarT (which generates adducts on single-stranded DNA) (Jankevicius et al., 2016) to probe the effect of mtDNA damage on mitochondrial dynamics in real-time. We find that mtDNA damage drives network fragmentation, likely due to a lowering in fusion rates arising from mitochondrial dysfunction. We further implicate a critical role for the exonuclease function of the mtDNA polymerase in mtDNA maintenance under damage. Our study reveals an intricate connection between mtDNA integrity, mitochondrial function and its role in regulating organelle organization and segregation.

121 **Results:**

122 **System to induce mitochondria-specific DNA damage**

123 To perturb mtDNA integrity and observe the resultant mitochondrial dynamics in real-time,
124 we developed an mtDNA-specific damage inducing system in *S. cerevisiae*. For this, we utilized
125 a bacterial toxin, DarT, that is part of a widely conserved DarT-DarG toxin-antitoxin system
126 (Jankevicius et al., 2016). DarT functions via transferring an ADP-ribosyl group on single-
127 stranded DNA using NAD+ as a substrate (Fig. 1A) and has been shown to generate DNA
128 damage-inducing adducts on the bacterial genome (likely via blocking replication progression)
129 (Lawarée et al., 2020). The adduct is attached to a thymidine within a 'TNTC' motif
130 (Jankevicius et al., 2016; Schuller et al., 2021)., which is present abundantly on the
131 mitochondrial genome.

132 We constructed a mitochondrial matrix-targeted DarT (derived from *T. aquaticus*), mtDarT,
133 via fusion of DarT to the first 69 amino acids of SU9 (subunit 9 of the F_1-F_0 ATPase) (Horie et
134 al., 2003). A 3XFlag-tag was added to the C-terminus of DarT, to enable verification of
135 expression as well as localization upon induction (Fig. S1A). mtDarT was expressed from a β-
136 estradiol inducible-promoter on a low copy plasmid (Louvion et al., 1993). This strategy was
137 employed to separately express a catalytically dead variant of DarT (DarTE160A), which
138 retains only negligible DarT activity (Jankevicius et al., 2016). We confirmed expression of
139 mtDarT, as well as mtDarTE160A via western blotting after 4 and 8hr of induction with 100nM
140 β-estradiol (Fig. S1B). Immunostaining using an anti-flag antibody revealed that the proteins
141 indeed localized to the mitochondria, marked using mitochondrially-targeted mNeonGreen
142 (mt-mNG) (Fig. 1B, S1C).

143 We next assessed the impact of mtDarT on cell growth, utilizing the ability of yeast cells to
144 show differential growth on fermentable/ non-fermentable carbon sources, based on their
145 mitochondrial activity (Ephrussi et al., 1955). Cells with impaired mitochondrial function are
146 able to survive on media containing a fermentable carbon source (albeit forming smaller,
147 'petite' colonies), due the ability of these cells to carry out glycolysis. However, such cells are
148 compromised for growth on non-fermentable carbon sources, where oxidative
149 phosphorylation (and hence complete mitochondrial function) is essential. When compared
150 with an empty vector control, we found that cells expressing mtDarT showed no associated

151 loss in viability on plates supplemented with dextrose (fermentable carbon source) (Fig. 1C).
152 These cells showed significant loss of viability in case of plates supplemented with glycerol
153 (non-fermentable carbon source) (Fig. 1C). Importantly, the growth defects observed were
154 mtDarT-specific and required the DNA adduct-forming catalytic function of DarT (Fig. 1C). This
155 supported the idea that mtDarT had mitochondria-specific action.

156 **mtDNA damage impacts mitochondrial organization and dynamics**

157 We next characterized the impact of mtDNA damage on mitochondrial organization and
158 function in glycolysis replete conditions. For this, we followed mitochondrial dynamics in cells
159 expressing Cox4-mCherry to track mitochondria in addition to mtDarT (or an empty vector
160 control). We classified the observed mitochondrial organizations into three distinct
161 categories: 'tubular', 'fragmented' and 'aggregate' (representative examples are shown in Fig.
162 2A). We found that the induction of mtDarT resulted in fragmentation of the mitochondrial
163 network (Fig. 2A-B), with an increase in percentage of cells with fragmented or aggregate
164 mitochondria. Indeed, cells carrying mtDarT displayed some perturbation to mitochondrial
165 organization even prior to induction, likely due to leaky expression from the vector (Fig. S2A).

166 We next followed the mtDarT-induced changes in mitochondrial organization over time via
167 measuring two features (Fig. 2C): a. the mean form factor (MFF) of mitochondria per cell, an
168 indicator of mitochondrial circularity (Chaudhry et al., 2020) and b. the number of discrete
169 mitochondria per cell. We plotted MFF and number of mitochondria for all cells as 2D density
170 plots, allowing us to visualize populations of cells having either tubular, fragmented or
171 aggregated mitochondria (Fig. 2C). We observed that control cells harboring an empty vector
172 largely populated MFF above 2 (predominantly tubular mitochondrial morphology) and
173 maximum density represented an intermediate between a tubular network and fragmented
174 state (Fig. 2D). This is as expected under unperturbed conditions, given the dynamic nature
175 of the mitochondria throughout the cell cycle (Shaw & Nunnari, 2002). In contrast, upon
176 mtDarT induction, mitochondria gradually transitioned from tubular (MFF >2) to fragmented/
177 aggregate states, having MFF <2 (Fig. 2D).

178 Organization of the mitochondrial network is regulated by a dedicated set of GTPases that
179 control mitochondrial membrane fission and fusion (Westermann, 2008). Hence, to assess

180 the contribution of changes in mitochondrial fission and/ or fusion upon mtDNA damage, we
181 followed mitochondrial dynamics via time-lapse microscopy. We imaged cells at 5 min
182 intervals for 40 min, after 4hr of damage exposure (Fig. 2E, S2B-C) and plotted density plots
183 as described above. Transition from tubular to fragmented states would reveal fission events,
184 while transition in the opposite direction (towards a tubular network) would be indicative of
185 fusion events.

186 To assess the impact of mtDNA damage on fission dynamics, we followed cells (control and
187 damage) with tubular mitochondrial networks at the start of imaging. We found that the rates
188 of mitochondrial fission (as assessed by transition of cells with MFF >2 to MFF <2), were
189 comparable between control and damage-treated cells (Fig. S2D). In line with this
190 observation, we did not find an increase in levels of the fission protein Dnm1 (Bleazard et al.,
191 1999) (Fig. S2E). Another mechanism for mitochondrial fission, independent of changes in the
192 levels of Dnm1, is via ERMES contact sites (Lewis et al., 2016). An increase in the number of
193 these contact sites (which can be imaged via tracking the number of Mdm34 localizations)
194 could lead to recruitment of Dnm1, thereby resulting in an increase in fission events.
195 However, we did not observe a significant increase in the number of ERMES contact sites in
196 cells facing damage (Fig. S2F).

197 Unlike the observed fission dynamics, cells facing mtDarT-induced damage had significantly
198 lower fusion events. When we followed individual cells over time, we found that mtDarT-
199 expressing cells with fragmented or aggregate mitochondrial organization did not display
200 dynamic reorganization towards a network morphology (Fig. 2E, S2C). Consistently, in
201 comparison to the control, cells expressing mtDarT were compromised in transitioning from
202 MFF <2 to MFF >2 (fragmented to tubular transition) and tended to maintain the density
203 distribution observed at the start of the experiment (Fig. 2F). The control cells on the other
204 hand were able to dynamically transition from MFF <2 to MFF>2 within the 40 min imaging
205 interval (Fig.2E-F).

206 Importantly, the above described effects of mtDarT were not cell size or cell cycle-stage
207 specific (as assessed by the presence and size of the bud), further underscoring the direct
208 impact of mtDNA damage on mitochondrial organization (Fig. S3A-B). Taken together, our
209 data suggest that under mtDNA damage, large scale reorganization of the mitochondrial
210 network likely arises from lowered mitochondrial membrane fusion rates.

211 **mtDNA damage results in mitochondrial dysfunction**

212 Given our observations on the impact of mtDNA damage on mitochondrial membrane fusion
213 dynamics, we wondered whether mitochondrial function was perturbed in these cells. We
214 thus measured mitochondrial membrane potential (ψ) via imaging TMRE (a membrane
215 potential sensitive dye) as a read-out for mitochondrial activity (Ludovico et al., 2001). We
216 observed a decrease in membrane potential in cells expressing mtDarT (Fig. 3A), similar to
217 impact of FCCP, a membrane decoupler which decreases ψ (Fig. S4A). This lowering in
218 membrane potential was observed even in mtDarT cells with reticular/ tubular networks,
219 suggesting that mitochondrial dysfunction upon mtDNA damage preceded changes in
220 mitochondrial organization and dynamics (Fig. S4B).

221 Specific lowering in mitochondrial fusion rates has been reported in cells with compromised
222 membrane potential (and hence dysfunction) (Duvezin-Caubet et al., 2006; Karbowski et al.,
223 2004; Legros et al., 2004; Twig et al., 2008). We thus hypothesized that mtDNA damage-
224 induced mitochondria with lowered membrane potential would display lower probability of
225 fusion, when compared with mitochondria with unperturbed membrane potential. To assess
226 this, we tracked mitochondrial dynamics (via mt-mNeongreen) in mtDarT-treated cells after
227 a brief pulse of TMRE staining (Fig. 3B-C). We then analysed the mean form factor and number
228 of mitochondria for cells specifically having MFF<2 (fragmented) along with their initial TMRE
229 fluorescence intensities, and asked whether these mitochondria were able to transition to a
230 tubular state. We observed that mitochondria with higher membrane potential, but
231 aggregate/ fragmented organization (MFF <2) were able to fuse into tubular mitochondrial
232 networks (MFF >2) (Fig. 3C-D). In contrast, fragmented mitochondria with lower membrane
233 potential were unable to do so during the course of imaging (Fig. 3C-D).

234 Our observations are consistent with the possibility that mtDNA damage results in
235 mitochondrial dysfunction (via reduced membrane potential), which in-turn affects
236 mitochondrial dynamics via impairing fusion.

237 **Changes in mitochondrial morphology accompany loss of mtDNA but not mitochondria**

238 We next assessed the effects of mtDarT damage on mtDNA, and whether the observed
239 mitochondrial dynamics contributed to clearance of damaged DNA/ dysfunctional
240 mitochondria. Following a previously-described method, we stained cells with SYBR Green I

241 to visualize mtDNA nucleoids (Jajoo et al., 2016) (Fig. 4A). In the control sample without
242 mtDNA damage, less than 2% cells had no detectable mtDNA foci ('ρ0' cells) at all time points
243 of imaging (Fig. 4B). In contrast, upon mtDarT induction, the percentage of ρ0 cells steadily
244 increased, with ~30% cells having no detectable foci post 8hr of damage induction (Fig. 4B).
245 Consistent with this, we also observed an overall decrease in the number of mtDNA foci per
246 cell upon mtDNA damage (Fig. S5A).

247 In some instance mitochondrial dysfunction (and associated fragmentation) has been shown
248 to occur in conjunction with mitophagy (Burman et al., 2017; Kleele et al., 2021). We thus
249 asked whether loss of mtDNA under damage was a result of clearance of dysfunctional
250 mitochondria. For this, we assessed the levels of two nuclear-encoded mitochondrial
251 proteins, Cox4 and Tom20, via western blot. We found that levels of these proteins did not
252 change significantly under damage conditions (Fig. 4C). We then measured mitochondrial
253 volume after induction of mtDarT (Fig. S5B) and found that here too, no significant changes
254 were observed over time. Consistent with the lack of change in mitochondrial content, we did
255 not observe an increase in mitophagy-associated marker, Atg8p (Torggler et al., 2017)
256 localizations. We also did not detect a significant difference in the amount of vacuolar
257 localization of Idh1 (Kanki & Klionsky, 2008) upon mtDarT-induction (Fig. S5C-D). This
258 suggested that an mtDNA-specific mechanism might be responsible for mtDNA clearance in
259 response to damage.

260 **Exonuclease activity of the mtDNA polymerase, Mip1, is essential for mtDNA maintenance**

261 In mammalian cells, the mtDNA replicative polymerase PolG can switch between synthesis
262 and degradation functions to clear out defective mtDNA (Nissanka et al., 2018; Peeva et al.,
263 2018). Evidence for such exonuclease function of the yeast homolog, Mip1, has also been
264 reported in conditions of starvation or oxidative stress (Medeiros et al., 2018). We hence
265 asked whether exonuclease activity could contribute to mtDNA clearance under mtDarT-
266 induced damage in our conditions. For this, we blocked the exonuclease activity of Mip1, via
267 mutating the catalytic site (D171A, E173A) responsible for its degradative function (Foury &
268 Vanderstraeten, 1992; Medeiros et al., 2018) (Fig. 5A) and assessed presence of mtDNA
269 nucleoids via SYBR Green I staining. Surprisingly, upon mtDarT induction, we observed that
270 Mip1 exonuclease deficient cells generated ρ0 cells significantly faster than wild type. As
271 shown earlier (Fig. 4B), 30% of wild type cells were ρ0 after 8hr of mtDarT induction. *mip1*$^{exo-}$

272 cells already generated ρ0 cells at a low frequency (~7%) in no damage conditions,
273 highlighting that inability to clear damaged mtDNA (in this case likely due to replication
274 errors) results in mtDNA loss in glucose replete growth environment. In line with this
275 observation, induction of mtDNA damage resulted in 60% cells becoming ρ0 post 8 hr of
276 mtDarT induction (Fig. 5B). Importantly, rapid mtDNA loss did not result in production of cells
277 devoid of mitochondria.

278 How do *mip1*$^{exo-}$ cells lose mtDNA in such a rapid manner under damage? We measured
279 budding events of wild type and mutant cells upon mtDNA damage and found them to be
280 comparable during the course of the experiment (3±1 budding events over 6 hr, for both wild
281 type and *mip1*$^{exo-}$ cells expressing mtDarT), ruling out the possibility of faster division rates in
282 the exonuclease mutant contributing to mtDNA loss over time. We next assessed
283 mitochondrial dynamics in the mutant. As seen in wild type cells, we found that mtDNA
284 damage resulted in significant changes to mitochondrial organization in case of exonuclease
285 deficient cells as well (Fig. S6A). Furthermore, in comparison to mtDarT-treated wild type
286 cells, we found that membrane potential was severely compromised in the mutant (Fig. S6B),
287 suggesting that these cells likely have significantly lowered mitochondrial membrane fusion
288 events. A potential outcome of enhanced mitochondrial dysfunction is a defect in the
289 segregation of mitochondria during division (McFaline-Figueroa et al., 2011). We thus
290 wondered whether this could impact partitioning of the mtDarT-induced damaged mtDNA.
291 Such partitioning defect would likely be more severe/ pronounced in the *mip1*$^{exo-}$ condition,
292 where defective mtDNA would accumulate due to lack of a clearance mechanism.

293 When we probed for mtDNA in these cells, we observed a significant proportion of cells with
294 mitochondria devoid of mtDNA in *mip1*$^{exo-}$ background (Fig 5C). We asked whether mtDNA
295 was differentially partitioned in these cells, resulting in generation of mitochondria devoid of
296 DNA as well. For this, we analysed mother-bud pairs after SYBR Green I staining, and
297 quantified the fraction of mtDNA foci in the bud (Fig. 5D). Consistent with previous reports
298 (Jajoo et al., 2016; Osman et al., 2015), we found that the amount of mtDNA partitioned in
299 the bud scaled with increasing bud area in control as well as wild type cells after mtDarT
300 induction (Fig. 5E). However, unlike wild type cells, there was significant heterogeneity in the
301 amount of mtDNA in the bud (across cell areas) in case of exonuclease deficient cells treated
302 with mtDarT, suggesting imprecise mtDNA partitioning (Fig. 5E), with several instances of

303 buds receiving no mtDNA (ρ0 daughter cells) (Fig. 5E). While we cannot rule out a role for
304 perturbed mtDNA replication in this case, such asymmetry in mtDNA partitioning can
305 contribute significantly to the rapid production of ρ0 cells in the exonuclease deficient
306 mutant. Taking these observations together, our results suggest that mitochondrial dynamics
307 could differentially impact damaged mtDNA segregation in conditions where defective
308 mtDNA clearance mechanisms are compromised, likely facilitating organelle segregation
309 independent of its DNA.

310

311

312 **Discussion:**

313 In this study, we describe a system to generate mtDNA-specific damage in *S. cerevisiae*. Using
314 a bacterial toxin DarT (Jankevicius et al., 2016), targeted to the mitochondria, we follow the
315 impact of mtDNA damage on mitochondrial organization, segregation and function. We find
316 that mtDNA damage affects mitochondrial function via compromising membrane potential.
317 This could be the causative force in mitochondrial reorganization by reduction in
318 mitochondrial membrane fusion events (Duvezin-Caubet et al., 2006; Karbowski et al., 2004;
319 Legros et al., 2004; Twig et al., 2008), facilitating selective segregation of mitochondria
320 without defective mtDNA (discussed below).
321 How cells sense and respond to mtDNA damage remains an outstanding and exciting
322 question. Previous studies have detected the presence of specific DNA repair enzymes
323 (include BER and recombination machinery) in the mitochondria (Alexeyev et al., 2013;
324 Boesch et al., 2011; Scheibye-Knudsen et al., 2015; Stevnsner et al., 2002). While some of
325 these pathways encode mitochondrially-targeted isoforms (Swartzlander et al., 2010), many
326 do not carry any known localization signal (Stuart et al., 2005; Thyagarajan et al., 1996). How
327 they localize to the mitochondria remains unclear, as is the importance of specific repair
328 pathways in mtDNA maintenance (Alexeyev et al., 2013; Scheibye-Knudsen et al., 2015).
329 Indeed, there are certain types of damages (such as UV-induced pyrimidine dimers) for which
330 active repair pathways have not been found in mitochondria (Clayton et al., 1974; Pascucci et
331 al., 1997). In such scenarios, where mtDNA damage becomes persistent, degradation of
332 damaged mtDNA copies has been proposed to occur (Alexeyev et al., 2013; Shokolenko et al.,
333 2013). Interestingly, this function is carried out by the exonuclease activity of the mtDNA
334 polymerase (Mip1 or PolG) itself (Nissanka et al., 2018; Peeva et al., 2018).
335 Our work further underscores a central role for defective mtDNA clearance via exonuclease
336 activity of the replicative polymerase under damage. We propose that Mip1 exonuclease
337 function is required for mtDNA degradation under damage and inability of cells to clear such
338 damaged mtDNA results in rapid generation of ρ0 cells in glucose replete conditions. Although
339 in unperturbed conditions, mtDNA and mitochondrial segregation may be coordinated (Jajoo
340 et al., 2016; Lewis et al., 2016; Osman et al., 2015), our observations thus support a role for
341 selective segregation of damaged mtDNA, in a manner that can result in partitioning of
342 mtDNA-less mitochondria in the daughter cells. Generation of cells devoid of mtDNA, without

343 significant loss of mitochondria would suggest cells can de-couple mtDNA and mitochondrial
344 partitioning and maintenance under conditions of damage, when complete mitochondrial
345 function may not be essential (such as in glycolytic conditions). Indeed, while mitochondria
346 cannot be made *de novo* (Westermann, 2014), ρ0 and ρ- cells in the environment could regain
347 and complement lost mtDNA, albeit with different proficiencies (Ling et al., 2019; Perlman,
348 1976).
349 It is interesting to note that mtDNA damage triggers rapid changes in mitochondrial
350 organization and segregation, and both the outcomes potentially stemming from
351 mitochondrial dysfunction. It would be important to understand how mtDNA damage causes
352 perturbations to mitochondrial function and how this in turn modulates rates of fusion. It is
353 possible that mtDNA damage can perturb levels of mitochondrially-encoded proteins such as
354 those part of the electron transport chain, which requires coordinated effort from nuclear
355 and mitochondrial genomes (Fontanesi et al., 2006; Herrmann & Funes, 2005). Separately,
356 studies have reported a direct impact of lowered membrane potential on differential
357 processing of Opa1 (a mitochondrial membrane fusion protein in mammals), affecting its
358 association with the mitochondrial membrane (Song et al., 2007). Although not probed in the
359 present study, it would be informative to assess function and levels of Fzo1 to determine if
360 known pathways of fusion are responsible for the observed dynamics in budding yeast.
361 The change in mitochondrial organization we report is consistent with observations in
362 mammalian cells, where mitochondrial network fragmentation has been seen to occur in
363 response to mtDNA damage (Ghosh et al., 2019). This suggests that mitochondrial
364 reorganization may be a universal response to mtDNA perturbation, as a fundamental quality
365 control mechanism to deal with mitochondrial dysfunction and regulate mtDNA/
366 mitochondrial segregation as well as clearance. Indeed in metazoans, mitochondrial fission
367 has been proposed to facilitate selective removal and degradation of mitochondria via
368 processes such as PINK-Parkin mediated mitophagy (Ni et al., 2015; Scheibye-Knudsen et al.,
369 2015).
370 Our results instead suggest that mitophagy does not play a significant role in the mtDNA
371 damage response in yeast and that quality control mechanisms likely act at the level of mtDNA
372 and its segregation (Fig. S5D). For example, previous reports have shown that budding yeast
373 cells segregate mitochondria asymmetrically based on the activity of the organelle (McFaline-
374 Figueroa et al., 2011; Vevea et al., 2014). Such asymmetry could also passively ensure

375 selective segregation of intact mtDNA copies to daughter cells. Indeed, recent studies
376 demonstrate selective removal or clearance of mutated mtDNA via sensing of local
377 mitochondrial activity as well as downregulation of mitochondrial fusion (Hill et al., 2014;
378 Jakubke et al., 2021; Lieber et al., 2019). It is tempting to speculate that in organisms like
379 budding yeast, that divide asymmetrically, the inability of dysfunctional mitochondria to fuse
380 with the rest of the mitochondrial network, along with selective segregation during division,
381 is the predominant mitochondrial quality control mechanism even in response to mtDNA
382 damage.
383 In sum, our study underscores: a. the impact of perturbations to mtDNA integrity on
384 mitochondrial dynamics and function; b. the importance of Mip1 exonuclease activity in
385 mtDNA maintenance under damage and c. the ability of cells to decouple mitochondrial and
386 mtDNA partitioning under mtDNA damage, with an emphasis on mitochondrial maintenance
387 even in the absence of mtDNA in glycolysis replete conditions. Indeed, the mtDarT system
388 developed here can provide a unique approach to enable future investigations on the
389 mechanisms that govern mtDNA-specific damage repair and recovery across diverse growth
390 conditions.

391 **Materials and methods**:

392 **Yeast strains and growth conditions**

393 A prototrophic strain CEN.PK of *Saccharomyces cerevisiae* was used as the background strain
394 in all the experiments (van Dijken et al., 2000). Plasmids, strains used in the study are listed
395 in Supplementary Table 1-3. Yeast cultures were grown in rich YP media (containing 2%
396 Peptone, 1% Yeast extract, and 2% Dextrose or 3% Glycerol as the carbon source) at 30°C with
397 200 rpm shaking with appropriate concentrations of antibiotics, as required. For all time-
398 course and time-lapse experiments, cells were transformed with the plasmids, and
399 transformants were inoculated in YPDextrose containing NAT and allowed to grow overnight.
400 These cultures were induced with β-estradiol at an O.D.~ 0.2. For induction, β-estradiol
401 (working stock- 50µM, prepared from a stock of 1mM in 100% molecular biology grade
402 ethanol) was added to a final concentration of 100nM, unless mentioned otherwise.

403 Yeast transformations were done using the LiAc method. For plasmid transformations, cells
404 were plated on YPDextrose plates containing appropriate concentrations of NAT and were
405 allowed to grow for 48 hr at 30°C. *mip1*$^{exo-}$ cells transformed with plasmids, were plated on
406 YPGlycerol plates containing appropriate concentrations of NAT and were allowed to grow
407 for 3 days at 30°C.

408 *mip1*$^{exo-}$ mutant was generated as described earlier (Medeiros et al., 2018). Briefly, we first
409 generated a *mip1Δ* strain which resulted in formation of $\boldsymbol{\rho}^0$ cells. We then introduced a copy
410 of the *mip1* gene containing the mutations D171A and E173A along with a hygromycin
411 selection cassette, at the same locus. Successful transformants containing the mutated copy
412 of the gene were then crossed with the wild type strain of the opposite mating type to
413 reintroduce mtDNA. The diploids were sporulated and tetrads were dissected to obtain $\boldsymbol{\rho}^+$
414 *mip1*$^{exo-}$ cells which were selected using hygromycin and the mating type was confirmed using
415 PCR primers specific for mating type locus. *mip1* gene was sequenced to confirm the presence
416 of the mutations. The strain was maintained on YPGlycerol post dissection to ensure selection
417 of only $\boldsymbol{\rho}^+$ cells; experiments were carried out in YPDextrose.

418

419

420 **mtDNA and mitochondrial staining**

421 For visualizing mtDNA, a previously described protocol was used (Jajoo et al., 2016). Briefly,
422 1ml of culture was pelleted and washed with 1X PBS. The supernatant was discarded and cells
423 were re- suspended in the residual buffer to give 50µl cell suspension. 0.5µl of undiluted SYBR
424 Green I (Invitrogen) was added to the cell suspension and mixed with gentle tapping. Cells
425 were immediately pelleted and supernatant was discarded. The pellets were washed with
426 1ml of 1X PBS. Cells were subsequently diluted to appropriate densities in 1X PBS before
427 imaging.

428 For visualizing the mitochondrial membrane potential, cells were pelleted and re-suspended
429 in 10ml of YPDextrose media (pre-warmed to 30°C) containing 1.5µM of TMRE. The cells were
430 incubated in the dark for 20 min in a shaker incubator (30°C, 200 rpm). Subsequently, cells
431 were pelleted down and washed with YPDextrose media in 2X the original volume of culture
432 used for staining. The cell pellets were resuspended to appropriate density in YPDextrose
433 prior to imaging. For time lapses, cells were stained with TMRE post 3.5 hr of induction, in
434 presence of 100nM β- estradiol. Following this, cells were washed and spotted on YPDextrose
435 pads for imaging.

436 **Fluorescence Microscopy**

437 Overnight cultures were allowed to grow till O.D.~0.2. At this O.D, mtDarT expression was
438 induced with 100nM β-estradiol. For time course experiments, samples were spotted on 1%
439 ultra-pure agarose water pads, and for time lapse experiments, samples were spotted on
440 YPDextrose pads with 100nM β-estradiol.

441 Microscopy was performed on a wide-field epifluorescence microscope (Eclipse Ti-2E, Nikon)
442 with a 63X oil immersion objective (plan apochromat objective with NA 1.41) and illumination
443 from pE4000 light source (CoolLED). The microscope was equipped with a motorized XYZ
444 stage and focus was maintained using an infrared-based Perfect Focusing System (Nikon).
445 Image acquisitions were done with Hamamatsu Orca Flash 4.0 camera using NIS-elements
446 software (version 5.1). For time-lapse imaging, samples were placed inside an OkoLab
447 incubation chamber maintained at 30°C and imaged at specific intervals for the indicated
448 period of time.

449 For SIM imaging, coverslips were sequentially washed in methanol and 100% ethanol and
450 flame dried prior to sample preparation. Cells were fixed in 3.7% para-formaldehyde (900µl
451 of cell suspension was added to 100µl of 37% para-formaldehyde) and then washed with 1X
452 PBS. Cells were then spotted on 1% ultra-pure agarose water pads and imaged. Samples were
453 imaged with Nikon 3D-SIM microscope equipped with an ANDOR iXon DU-897 EMCCD camera
454 (512X512), 100X ApoTIRF 1.49 NA oil objective with Coherent Sapphire 561nm solid state
455 laser as the light source. Image reconstruction was done using NIS elements software
456 (Illumination modulation contrast – Auto, High resolution noise suppression – 1X, Out of focus
457 blur suppression – 0.25). During acquisition, 800ms exposure for COX4-mCherry with 20%
458 laser power, 150 EM gain and 0.3 µm step size was used.

459 **Image analysis**

460 All image analysis was performed using MATLAB and Fiji (ImageJ) (Schindelin et al., 2012).
461 Mitochondrial analysis was done on 2D maximum projections of z-stacks and images were
462 deconvolved using NIS-elements AR software (Richardson-Lucy algorithm with 60-iterations).
463 Cell segmentation was performed using a MATLAB algorithm (Doncic et al., 2013). Cell
464 outlines were extracted from .mat output files from the algorithm and then ROIs were
465 obtained using Fiji. For segmentation of mitochondria, a custom pipeline was set up in Fiji
466 (briefly involving a. Background subtraction (Rolling ball radius: 50 pixels). b. Sigma Filter Plus
467 (radius =1 pixel, use pixels within = 2 sigmas, Minimum pixel fraction = 0.2). c. Enhanced Local
468 Contrast (CLAHE) (Blocksize = 64, histogram = 256, maximum = 2). d. Tubeness filter (sigma
469 =1.000). e. Images converted to 8-bit. f. Thresholding (10,255) (Minimum threshold was
470 adjusted between 8-15 depending on the quality of segmentation). g. Images converted to
471 mask, Despeckled and Remove outliers (Radius =2, threshold =50)) and the mitochondrial
472 descriptors (Mean form factor, mtArea, Number of mitochondria on per cell basis) were
473 obtained using Mitochondrial analyzer (Chaudhry et al., 2020). Whole cell TMRE intensity was
474 analyzed from maximum projections using 'Measure' in Fiji. For Fig. 2A, cells were manually
475 binned into three morphological categories and buds were excluded from the analysis. For
476 detection of mtDNA foci post SYBR Green I staining, 3D maxima finder plugin (part of the 3D
477 ImageJSuite) in ImageJ was utilized. Since cells with less/without any mtDNA also show
478 nuclear DNA staining, we manually scored these cells post segmentation to account for
479 detection of foci due to nuclear staining. For mtDNA analysis in mother vs bud, pairs without

480 any mtDNA foci (in both cell types) were removed. Mitochondrial volume was analyzed using
481 Mitograph (Rafelski et al., 2012; Viana et al., 2015).

482 **Western blotting**

483 Transformants were inoculated in 100-120 ml of YPDextrose with appropriate concentrations
484 of NAT. Cultures were induced with 100nM β-estradiol at an O.D ~ 0.2. Cells were harvested
485 and protein isolation was performed using the Trichloroacetic acid (TCA) extraction method.
486 Pellets were resuspended in 300µl of 10% TCA and lysed by bead beating thrice. The
487 precipitates were resuspended in 200µl of SDS-Glycerol buffer (7.3% SDS, 29.1% glycerol and
488 83.3 mM Tris base) and boiled at 95°C for 10 min with frequent vortexing. The lysate was
489 precipitated and the supernatant was obtained containing protein. Estimation of protein
490 concentration was done using the BCA estimation method using GBioSciences assay kit. The
491 assay was performed in disposable cuvettes, where 5µl was mixed with 1ml Solution A and
492 20µl of Solution B and incubated at 30°C for 30 min. The absorbance was recorded at 565nm.
493 Equal amounts of protein were then loaded on a polyacrylamide gel. For Cox4-mCherry,
494 Dnm1-HA blots 8-10% gels were used. PVDF membranes were used for blotting, which were
495 probed with anti-mCherry (1:5000), anti-HA (1:5000) antibodies. HRP conjugated secondary
496 antibodies were used (1:5000) for western blotting and blots were developed using
497 SuperSignal West PICO PLUS or FEMTO PLUS chemiluminescent substrate. Equal amount of
498 proteins was loaded on a separate gel and stained with Coomassie Brillian Blue as a loading
499 control.

500 **Immunocytochemistry**

501 Mid-log phase cells were harvested and fixed in 1ml of 4% paraformaldehyde for 30 min at
502 room temperature. After washing the cells twice with a phosphate-sorbitol buffer (0.1 M
503 KPO4 and 1x in 0.1 M KPO4/1.2 M sorbitol), the pellet was resuspended in 1 ml of 0.1M
504 KPO4/1.2M sorbitol. Cells were then spheroplasted with 10mg/ml Zymolyase for 10-30 min
505 in presence of β-mercaptoethanol. Spheroplasting was checked by imaging cells on the
506 microscope. For imaging, slides/dishes were prepared by washing in chilled methanol and
507 95% ethanol. Slides were then coated with 0.1% Poly-L lysine for 5-10 min and then washed
508 thrice with dH2O. 15µl of spheroplast suspension was placed in each well for 5-10 min at

509 room temperature and then aspirated, and immediately plunged into ice cold methanol for
510 5-6 min and then in cold acetone for 30 sec. Post air drying, 25µl of PBS-BSA was used for
511 blocking. Primary antibody probing was done following 30 min of blocking, for 1 hr. After 5
512 washes with PBS-BSA, secondary antibody was added and incubated for 1-2 hr in a humid
513 chamber in the dark. The wells were again washed with PBS-BSA five times (each wash for 10
514 min) and then twice with only PBS. Slides were mounted with mounted media (Slowfade DAPI
515 reagent) and imaged.

516

517

Acknowledgements

The authors are grateful to Dr. Ivan Ahel for sharing bacterial DarT and DarG constructs and Afroze Chimthanawala for assistance with SIM imaging. The authors thank Dr. Sunil Laxman and members of the AB and SL labs for helpful discussions and feedback on the manuscript. This work was supported by fellowships from TIFR (ND), CSIR (AS) as well as grants from HFSP CDA (00051/ 2017-C) (AB) and intramural funding from NCBS-TIFR (AB).

Author contributions

ND: conception of project, experimental design, generation of tools and reagents, execution of experiments, data analysis, writing of manuscript. AS: experimental design, generation of tools and reagents, execution of experiments, data analysis, editing of manuscript. AB: conception of project, project supervision, experimental design and writing of manuscript.

Declaration of interests

The authors declare no competing interests.

535 **References**

536 Alexeyev, M., Shokolenko, I., Wilson, G., & LeDoux, S. (2013). The Maintenance of
537 Mitochondrial DNA Integrity—Critical Analysis and Update. *Cold Spring Harbor Perspectives*
538 *in Biology*, *5*(5). https://doi.org/10.1101/cshperspect.a012641
539
540 Bagamery, L. E., Justman, Q. A., Garner, E. C., & Murray, A. W. (2020). A Putative Bet-Hedging
541 Strategy Buffers Budding Yeast against Environmental Instability. *Current Biology*, *30*(23),
542 4563-4578.e4. https://doi.org/10.1016/j.cub.2020.08.092
543
544 Bleazard, W., McCaffery, J. M., King, E. J., Bale, S., Mozdy, A., Tieu, Q., Nunnari, J., & Shaw, J.
545 M. (1999). The dynamin-related GTPase Dnm1 regulates mitochondrial fission in yeast.
546 *Nature Cell Biology*, *1*(5), 298–304. https://doi.org/10.1038/13014
547
548 Boesch, P., Weber-Lotfi, F., Ibrahim, N., Tarasenko, V., Cosset, A., Paulus, F., Lightowlers, R.
549 N., & Dietrich, A. (2011). DNA repair in organelles: Pathways, organization, regulation,
550 relevance in disease and aging. *Biochimica et Biophysica Acta (BBA) - Molecular Cell Research*,
551 *1813*(1), 186–200. https://doi.org/10.1016/j.bbamcr.2010.10.002
552
553 Brown, T. A., Tkachuk, A. N., Shtengel, G., Kopek, B. G., Bogenhagen, D. F., Hess, H. F., &
554 Clayton, D. A. (2011). Superresolution Fluorescence Imaging of Mitochondrial Nucleoids
555 Reveals Their Spatial Range, Limits, and Membrane Interaction. *Molecular and Cellular*
556 *Biology*. https://doi.org/10.1128/MCB.05694-11
557
558 Burman, J. L., Pickles, S., Wang, C., Sekine, S., Vargas, J. N. S., Zhang, Z., Youle, A. M., Nezich,
559 C. L., Wu, X., Hammer, J. A., & Youle, R. J. (2017). Mitochondrial fission facilitates the selective
560 mitophagy of protein aggregates. *Journal of Cell Biology*, *216*(10), 3231–3247.
561 https://doi.org/10.1083/jcb.201612106
562
563 Busch, K. B., Kowald, A., & Spelbrink, J. N. (2014). Quality matters: How does mitochondrial
564 network dynamics and quality control impact on mtDNA integrity? *Philosophical Transactions*
565 *of the Royal Society B: Biological Sciences*, *369*(1646), 20130442.
566 https://doi.org/10.1098/rstb.2013.0442
567
568 Chaudhry, A., Shi, R., & Luciani, D. S. (2020). A pipeline for multidimensional confocal analysis
569 of mitochondrial morphology, function, and dynamics in pancreatic β-cells. *American Journal*
570 *of Physiology-Endocrinology and Metabolism*, *318*(2), E87–E101.
571 https://doi.org/10.1152/ajpendo.00457.2019
572
573 Chen, X. J., & Butow, R. A. (2005). The organization and inheritance of the mitochondrial
574 genome. *Nature Reviews Genetics*, *6*(11), 815–825. https://doi.org/10.1038/nrg1708
575
576 Clayton, D. A., Doda, J. N., & Friedberg, E. C. (1974). The Absence of a Pyrimidine Dimer Repair
577 Mechanism in Mammalian Mitochondria. *Proceedings of the National Academy of Sciences of*
578 *the United States of America*, *71*(7), 2777–2781.
579
580 Detmer, S. A., & Chan, D. C. (2007). Functions and dysfunctions of mitochondrial dynamics.
581 *Nature Reviews Molecular Cell Biology*, *8*(11), 870–879. https://doi.org/10.1038/nrm2275

582
583 Doncic, A., Eser, U., Atay, O., & Skotheim, J. M. (2013). An Algorithm to Automate Yeast
584 Segmentation and Tracking. *PLOS ONE*, *8*(3), e57970.
585 https://doi.org/10.1371/journal.pone.0057970
586
587 Duvezin-Caubet, S., Jagasia, R., Wagener, J., Hofmann, S., Trifunovic, A., Hansson, A., Chomyn,
588 A., Bauer, M. F., Attardi, G., Larsson, N.-G., Neupert, W., & Reichert, A. S. (2006). Proteolytic
589 Processing of OPA1 Links Mitochondrial Dysfunction to Alterations in Mitochondrial
590 Morphology *. *Journal of Biological Chemistry*, *281*(49), 37972–37979.
591 https://doi.org/10.1074/jbc.M606059200
592
593 Ephrussi, B., de Margerie-Hottinguer, H., & Roman, H. (1955). SUPPRESSIVENESS: A NEW
594 FACTOR IN THE GENETIC DETERMINISM OF THE SYNTHESIS OF RESPIRATORY ENZYMES IN
595 YEAST. *Proceedings of the National Academy of Sciences of the United States of America*,
596 *41*(12), 1065–1071.
597
598 Farge, G., Laurens, N., Broekmans, O. D., van den Wildenberg, S. M. J. L., Dekker, L. C. M.,
599 Gaspari, M., Gustafsson, C. M., Peterman, E. J. G., Falkenberg, M., & Wuite, G. J. L. (2012).
600 Protein sliding and DNA denaturation are essential for DNA organization by human
601 mitochondrial transcription factor A. *Nature Communications*, *3*(1), 1013.
602 https://doi.org/10.1038/ncomms2001
603
604 Fontanesi, F., Soto, I. C., Horn, D., & Barrientos, A. (2006). Assembly of mitochondrial
605 cytochrome c-oxidase, a complicated and highly regulated cellular process. *American Journal*
606 *of Physiology-Cell Physiology*, *291*(6), C1129–C1147.
607 https://doi.org/10.1152/ajpcell.00233.2006
608
609 Foury, F., & Vanderstraeten, S. (1992). Yeast mitochondrial DNA mutators with deficient
610 proofreading exonucleolytic activity. *The EMBO Journal*, *11*(7), 2717–2726.
611
612 Ghosh, A., Bhattacharjee, S., Chowdhuri, S. P., Mallick, A., Rehman, I., Basu, S., & Das, B. B.
613 (2019). SCAN1-TDP1 trapping on mitochondrial DNA promotes mitochondrial dysfunction and
614 mitophagy. *Science Advances*, *5*(11), eaax9778. https://doi.org/10.1126/sciadv.aax9778
615
616 Hahn, A., & Zuryn, S. (2019). The Cellular Mitochondrial Genome Landscape in Disease. *Trends*
617 *in Cell Biology*, *29*(3), 227–240. https://doi.org/10.1016/j.tcb.2018.11.004
618
619 Herrmann, J. M., & Funes, S. (2005). Biogenesis of cytochrome oxidase-sophisticated
620 assembly lines in the mitochondrial inner membrane. *Gene*, *354*, 43–52.
621 https://doi.org/10.1016/j.gene.2005.03.017
622
623 Hill, J. H., Chen, Z., & Xu, H. (2014). Selective propagation of functional mitochondrial DNA
624 during oogenesis restricts the transmission of a deleterious mitochondrial variant. *Nature*
625 *Genetics*, *46*(4), 389–392. https://doi.org/10.1038/ng.2920
626
627 Horie, C., Suzuki, H., Sakaguchi, M., & Mihara, K. (2003). Targeting and Assembly of
628 Mitochondrial Tail-anchored Protein Tom5 to the TOM Complex Depend on a Signal Distinct

from That of Tail-anchored Proteins Dispersed in the Membrane *. *Journal of Biological Chemistry*, *278*(42), 41462–41471. https://doi.org/10.1074/jbc.M307047200

Jajoo, R., Jung, Y., Huh, D., Viana, M. P., Rafelski, S. M., Springer, M., & Paulsson, J. (2016). Accurate concentration control of mitochondria and nucleoids. *Science (New York, N.Y.)*, *351*(6269), 169–172. https://doi.org/10.1126/science.aaa8714

Jakubke, C., Roussou, R., Maiser, A., Schug, C., Thoma, F., Bunk, D., Hörl, D., Leonhardt, H., Walter, P., Klecker, T., & Osman, C. (n.d.). Cristae-dependent quality control of the mitochondrial genome. *Science Advances*, *7*(36), eabi8886. https://doi.org/10.1126/sciadv.abi8886

Jankevicius, G., Ariza, A., Ahel, M., & Ahel, I. (2016). The Toxin-Antitoxin System DarTG Catalyzes Reversible ADP-Ribosylation of DNA. *Molecular Cell*, *64*(6), 1109–1116. https://doi.org/10.1016/j.molcel.2016.11.014

Jiao, H., Jiang, D., Hu, X., Du, W., Ji, L., Yang, Y., Li, X., Sho, T., Wang, X., Li, Y., Wu, Y.-T., Wei, Y.-H., Hu, X., & Yu, L. (2021). Mitocytosis, a migrasome-mediated mitochondrial quality-control process. *Cell*, *184*(11), 2896-2910.e13. https://doi.org/10.1016/j.cell.2021.04.027

Jin, S. M., & Youle, R. J. (2012). PINK1- and Parkin-mediated mitophagy at a glance. *Journal of Cell Science*, *125*(4), 795–799. https://doi.org/10.1242/jcs.093849

Kanki, T., & Klionsky, D. J. (2008). Mitophagy in Yeast Occurs through a Selective Mechanism. *The Journal of Biological Chemistry*, *283*(47), 32386–32393. https://doi.org/10.1074/jbc.M802403200

Karbowski, M., Arnoult, D., Chen, H., Chan, D. C., Smith, C. L., & Youle, R. J. (2004). Quantitation of mitochondrial dynamics by photolabeling of individual organelles shows that mitochondrial fusion is blocked during the Bax activation phase of apoptosis. *Journal of Cell Biology*, *164*(4), 493–499. https://doi.org/10.1083/jcb.200309082

Kleele, T., Rey, T., Winter, J., Zaganelli, S., Mahecic, D., Perreten Lambert, H., Ruberto, F. P., Nemir, M., Wai, T., Pedrazzini, T., & Manley, S. (2021). Distinct fission signatures predict mitochondrial degradation or biogenesis. *Nature*, *593*(7859), 435–439. https://doi.org/10.1038/s41586-021-03510-6

Laporte, D., Gouleme, L., Jimenez, L., Khemiri, I., & Sagot, I. (2018). Mitochondria reorganization upon proliferation arrest predicts individual yeast cell fate. *ELife*, *7*, e35685. https://doi.org/10.7554/eLife.35685

Lawarée, E., Jankevicius, G., Cooper, C., Ahel, I., Uphoff, S., & Tang, C. M. (2020). DNA ADP-Ribosylation Stalls Replication and Is Reversed by RecF-Mediated Homologous Recombination and Nucleotide Excision Repair. *Cell Reports*, *30*(5), 1373-1384.e4. https://doi.org/10.1016/j.celrep.2020.01.014

675 Legros, F., Malka, F., Frachon, P., Lombès, A., & Rojo, M. (2004). Organization and dynamics
676 of human mitochondrial DNA. *Journal of Cell Science*, *117*(13), 2653–2662.
677 https://doi.org/10.1242/jcs.01134
678
679 Lewis, S. C., Uchiyama, L. F., & Nunnari, J. (2016). ER-mitochondria contacts couple mtDNA
680 synthesis with mitochondrial division in human cells. *Science*, *353*(6296).
681 https://doi.org/10.1126/science.aaf5549
682
683 Lieber, T., Jeedigunta, S. P., Palozzi, J. M., Lehmann, R., & Hurd, T. R. (2019). Mitochondrial
684 fragmentation drives selective removal of deleterious mtDNA in the germline. *Nature*,
685 *570*(7761), 380–384. https://doi.org/10.1038/s41586-019-1213-4
686
687 Ling, F., Bradshaw, E., & Yoshida, M. (2019). Prevention of mitochondrial genomic instability
688 in yeast by the mitochondrial recombinase Mhr1. *Scientific Reports*, *9*(1), 5433.
689 https://doi.org/10.1038/s41598-019-41699-9
690
691 Louvion, J. F., Havaux-Copf, B., & Picard, D. (1993). Fusion of GAL4-VP16 to a steroid-binding
692 domain provides a tool for gratuitous induction of galactose-responsive genes in yeast. *Gene*,
693 *131*(1), 129–134. https://doi.org/10.1016/0378-1119(93)90681-r
694
695 Ludovico, P., Sansonetty, F., & Côrte-Real, M. (2001). Assessment of mitochondrial membrane
696 potential in yeast cell populations by flow cytometry. *Microbiology (Reading, England)*, *147*(Pt
697 12), 3335–3343. https://doi.org/10.1099/00221287-147-12-3335
698
699 McFaline-Figueroa, J. R., Vevea, J., Swayne, T. C., Zhou, C., Liu, C., Leung, G., Boldogh, I. R., &
700 Pon, L. A. (2011). Mitochondrial quality control during inheritance is associated with lifespan
701 and mother-daughter age asymmetry in budding yeast. *Aging Cell*, *10*(5), 885–895.
702 https://doi.org/10.1111/j.1474-9726.2011.00731.x
703
704 Medeiros, T. C., Thomas, R. L., Ghillebert, R., & Graef, M. (2018). Autophagy balances mtDNA
705 synthesis and degradation by DNA polymerase POLG during starvation. *Journal of Cell Biology*,
706 *217*(5), 1601–1611. https://doi.org/10.1083/jcb.201801168
707
708 Nakada, K., Inoue, K., Ono, T., Isobe, K., Ogura, A., Goto, Y. I., Nonaka, I., & Hayashi, J. I. (2001).
709 Inter-mitochondrial complementation: Mitochondria-specific system preventing mice from
710 expression of disease phenotypes by mutant mtDNA. *Nature Medicine*, *7*(8), 934–940.
711 https://doi.org/10.1038/90976
712
713 Ni, H.-M., Williams, J. A., & Ding, W.-X. (2015). Mitochondrial dynamics and mitochondrial
714 quality control. *Redox Biology*, *4*, 6–13. https://doi.org/10.1016/j.redox.2014.11.006
715
716 Nissanka, N., Bacman, S. R., Plastini, M. J., & Moraes, C. T. (2018). The mitochondrial DNA
717 polymerase gamma degrades linear DNA fragments precluding the formation of deletions.
718 *Nature Communications*, *9*(1), 2491. https://doi.org/10.1038/s41467-018-04895-1
719
720 Osman, C., Noriega, T. R., Okreglak, V., Fung, J. C., & Walter, P. (2015). Integrity of the yeast
721 mitochondrial genome, but not its distribution and inheritance, relies on mitochondrial fission

and fusion. *Proceedings of the National Academy of Sciences of the United States of America*, *112*(9), E947–E956. https://doi.org/10.1073/pnas.1501737112

Pascucci, B., Versteegh, A., van Hoffen, A., van Zeeland, A. A., Mullenders, L. H., & Dogliotti, E. (1997). DNA repair of UV photoproducts and mutagenesis in human mitochondrial DNA. *Journal of Molecular Biology*, *273*(2), 417–427. https://doi.org/10.1006/jmbi.1997.1268

Peeva, V., Blei, D., Trombly, G., Corsi, S., Szukszto, M. J., Rebelo-Guiomar, P., Gammage, P. A., Kudin, A. P., Becker, C., Altmüller, J., Minczuk, M., Zsurka, G., & Kunz, W. S. (2018). Linear mitochondrial DNA is rapidly degraded by components of the replication machinery. *Nature Communications*, *9*(1), 1727. https://doi.org/10.1038/s41467-018-04131-w

Perlman, P. S. (1976). Genetic analysis of petite mutants of Saccharomyces cerevisiae: Transmissional types. *Genetics*, *82*(4), 645–663. https://doi.org/10.1093/genetics/82.4.645

Pickles, S., Vigié, P., & Youle, R. J. (2018). Mitophagy and Quality Control Mechanisms in Mitochondrial Maintenance. *Current Biology: CB*, *28*(4), R170–R185. https://doi.org/10.1016/j.cub.2018.01.004

Rafelski, S. M., Viana, M. P., Zhang, Y., Chan, Y.-H. M., Thorn, K. S., Yam, P., Fung, J. C., Li, H., Costa, L. da F., & Marshall, W. F. (2012). Mitochondrial Network Size Scaling in Budding Yeast. *Science (New York, N.Y.)*, *338*(6108), 822–824. https://doi.org/10.1126/science.1225720

Ramos, E. S., Motori, E., Brüser, C., Kühl, I., Yeroslaviz, A., Ruzzenente, B., Kauppila, J. H. K., Busch, J. D., Hultenby, K., Habermann, B. H., Jakobs, S., Larsson, N.-G., & Mourier, A. (2019). Mitochondrial fusion is required for regulation of mitochondrial DNA replication. *PLOS Genetics*, *15*(6), e1008085. https://doi.org/10.1371/journal.pgen.1008085

Richter, C. (1995). Oxidative damage to mitochondrial DNA and its relationship to ageing. *The International Journal of Biochemistry & Cell Biology*, *27*(7), 647–653. https://doi.org/10.1016/1357-2725(95)00025-K

Scheibye-Knudsen, M., Fang, E. F., Croteau, D. L., Wilson, D. M., & Bohr, V. A. (2015). Protecting the Mitochondrial Powerhouse. *Trends in Cell Biology*, *25*(3), 158–170. https://doi.org/10.1016/j.tcb.2014.11.002

Schindelin, J., Arganda-Carreras, I., Frise, E., Kaynig, V., Longair, M., Pietzsch, T., Preibisch, S., Rueden, C., Saalfeld, S., Schmid, B., Tinevez, J.-Y., White, D. J., Hartenstein, V., Eliceiri, K., Tomancak, P., & Cardona, A. (2012). Fiji: An open-source platform for biological-image analysis. *Nature Methods*, *9*(7), 676–682. https://doi.org/10.1038/nmeth.2019

Schuller, M., Butler, R. E., Ariza, A., Tromans-Coia, C., Jankevicius, G., Claridge, T. D. W., Kendall, S. L., Goh, S., Stewart, G. R., & Ahel, I. (2021). Molecular basis for DarT ADP-ribosylation of a DNA base. *Nature*, *596*(7873), 597–602. https://doi.org/10.1038/s41586-021-03825-4

Scott, I., & Youle, R. J. (2010). Mitochondrial fission and fusion. *Essays in Biochemistry*, *47*, 85–98. https://doi.org/10.1042/bse0470085

Shaw, J. M., & Nunnari, J. (2002). Mitochondrial dynamics and division in budding yeast. *Trends in Cell Biology*, *12*(4), 178–184.

Shokolenko, I. N., Wilson, G. L., & Alexeyev, M. F. (2013). Persistent damage induces mitochondrial DNA degradation. *DNA Repair*, *12*(7), 488–499. https://doi.org/10.1016/j.dnarep.2013.04.023

Song, Z., Chen, H., Fiket, M., Alexander, C., & Chan, D. C. (2007). OPA1 processing controls mitochondrial fusion and is regulated by mRNA splicing, membrane potential, and Yme1L. *Journal of Cell Biology*, *178*(5), 749–755. https://doi.org/10.1083/jcb.200704110

Stevnsner, T., Thorslund, T., de Souza-Pinto, N. C., & Bohr, V. A. (2002). Mitochondrial repair of 8-oxoguanine and changes with aging. *Experimental Gerontology*, *37*(10–11), 1189–1196. https://doi.org/10.1016/s0531-5565(02)00142-0

Stuart, J. A., Mayard, S., Hashiguchi, K., Souza-Pinto, N. C., & Bohr, V. A. (2005). Localization of mitochondrial DNA base excision repair to an inner membrane-associated particulate fraction. *Nucleic Acids Research*, *33*(12), 3722–3732. https://doi.org/10.1093/nar/gki683

Swartzlander, D. B., Griffiths, L. M., Lee, J., Degtyareva, N. P., Doetsch, P. W., & Corbett, A. H. (2010). Regulation of base excision repair: Ntg1 nuclear and mitochondrial dynamic localization in response to genotoxic stress. *Nucleic Acids Research*, *38*(12), 3963–3974. https://doi.org/10.1093/nar/gkq108

Taylor, R. W., & Turnbull, D. M. (2005). Mitochondrial DNA mutations in human disease. *Nature Reviews Genetics*, *6*(5), 389–402. https://doi.org/10.1038/nrg1606

Thyagarajan, B., Padua, R. A., & Campbell, C. (1996). Mammalian mitochondria possess homologous DNA recombination activity. *The Journal of Biological Chemistry*, *271*(44), 27536–27543. https://doi.org/10.1074/jbc.271.44.27536

Torggler, R., Papinski, D., & Kraft, C. (2017). Assays to Monitor Autophagy in Saccharomyces cerevisiae. *Cells*, *6*(3), E23. https://doi.org/10.3390/cells6030023

Twig, G., Elorza, A., Molina, A. J. A., Mohamed, H., Wikstrom, J. D., Walzer, G., Stiles, L., Haigh, S. E., Katz, S., Las, G., Alroy, J., Wu, M., Py, B. F., Yuan, J., Deeney, J. T., Corkey, B. E., & Shirihai, O. S. (2008). Fission and selective fusion govern mitochondrial segregation and elimination by autophagy. *The EMBO Journal*, *27*(2), 433–446. https://doi.org/10.1038/sj.emboj.7601963

van Dijken, J. P., Bauer, J., Brambilla, L., Duboc, P., Francois, J. M., Gancedo, C., Giuseppin, M. L. F., Heijnen, J. J., Hoare, M., Lange, H. C., Madden, E. A., Niederberger, P., Nielsen, J., Parrou, J. L., Petit, T., Porro, D., Reuss, M., van Riel, N., Rizzi, M., … Pronk, J. T. (2000). An interlaboratory comparison of physiological and genetic properties of four Saccharomyces

814 cerevisiae strains. *Enzyme and Microbial Technology*, *26*(9), 706–714.
815 https://doi.org/10.1016/S0141-0229(00)00162-9
816
817 Vevea, J. D., Swayne, T. C., Boldogh, I. R., & Pon, L. A. (2014). Inheritance of the fittest
818 mitochondria in yeast. *Trends in Cell Biology*, *24*(1).
819 https://doi.org/10.1016/j.tcb.2013.07.003
820
821 Viana, M. P., Lim, S., & Rafelski, S. M. (2015). Quantifying mitochondrial content in living cells.
822 *Methods in Cell Biology*, *125*, 77–93. https://doi.org/10.1016/bs.mcb.2014.10.003
823
824 Wallace, D. C. (2010). Mitochondrial DNA mutations in disease and aging. *Environmental and*
825 *Molecular Mutagenesis*, *51*(5), 440–450. https://doi.org/10.1002/em.20586
826 Westermann, B. (2008). Molecular Machinery of Mitochondrial Fusion and Fission. *Journal of*
827 *Biological Chemistry*, *283*(20), 13501–13505. https://doi.org/10.1074/jbc.R800011200
828
829 Westermann, B. (2010). Mitochondrial fusion and fission in cell life and death. *Nature Reviews*
830 *Molecular Cell Biology*, *11*(12), 872–884. https://doi.org/10.1038/nrm3013
831
832 Westermann, B. (2014). Mitochondrial inheritance in yeast. *Biochimica Et Biophysica Acta*,
833 *1837*(7), 1039–1046. https://doi.org/10.1016/j.bbabio.2013.10.005
834
835 Yakes, F. M., & Van Houten, B. (1997). Mitochondrial DNA damage is more extensive and
836 persists longer than nuclear DNA damage in human cells following oxidative stress.
837 *Proceedings of the National Academy of Sciences of the United States of America*, *94*(2), 514–
838 519. https://doi.org/10.1073/pnas.94.2.514
839
840 Zhang, Y., Wang, Z.-H., Liu, Y., Chen, Y., Sun, N., Gucek, M., Zhang, F., & Xu, H. (2019). PINK1
841 Inhibits Local Protein Synthesis to Limit Transmission of Deleterious Mitochondrial DNA
842 Mutations. *Molecular Cell*, *73*(6), 1127-1137.e5.
843 https://doi.org/10.1016/j.molcel.2019.01.013
844

845 **Main Figure legends**

846 **Figure 1: System to induce mitochondria-specific DNA damage.** (A). Schematic representing
847 expression and localization of mtDarT on addition of β-estradiol (Left panel); Diagrammatic
848 representation of ADP-ribosylation of single stranded DNA in presence of DarT and NAD+
849 (Right panel). (B). Immunostaining for FLAG-tagged mtDarT/TE160A in cells expressing
850 mitochondrially-targeted mNeongreen. Intensity line profiles for mtDarT and mNeonGreen
851 are shown on the right. (C). Cell survival under increasing concentrations of β-estradiol on
852 plates containing either dextrose or glycerol as a carbon source; cells were transformed with
853 plasmids expressing mtDarT/TE160A or empty vector as a control. (Scale bar-5µm, white
854 dotted lines mark cell outlines, here and in all other images)

855 **Figure 2: mtDNA damage impacts mitochondrial organization and dynamics.** (A).
856 Representative cells showing three categories of mitochondrial morphologies observed (left
857 panel); Percentage of cells in each category in control (empty vector) or mtDarT cells after 8
858 hr of induction (Mean ± SD from three biological replicates, n>150 in each replicate) (right
859 panel). (B). Cells expressing Cox4::mCherry imaged in widefield and SIM mode, with
860 representative cells showing tubular and fragmented mitochondrial morphologies after 6 hr
861 of induction with 100nM β-estradiol. (C). Two parameters: - Mean form factor (MFF) and
862 number of mitochondria are used to quantify mitochondrial morphologies in the population.
863 Details on calculation of MFF is provided, along with a diagrammatic representation of
864 possible mitochondrial organizations observed in the 2D density plots (D). Density plots with
865 Mean form factor and number of mitochondria over time; n>680 in each plot, from 3
866 biological replicates. (E). Montage of cells with Cox4::mCherry, imaged every 5 min for 40 min,
867 after 4 hr of induction with β-estradiol; mitochondrial morphology at the start of the
868 experiment is indicated (F). Density plots with Mean form factor and number of mitochondria
869 over time, plotted for cells starting with MFF<2 at the beginning of time lapse; n=84 for empty
870 vector, n= 151 for mtDarT pooled from 3 biological replicates.

871 **Figure 3: mtDNA damage results in mitochondrial dysfunction.** (A). Representative images
872 of cells expressing Cox4::GFP and stained with TMRE after 8 hr of induction with β-estradiol
873 (left panel). Total TMRE intensity normalized to cell area is plotted (n>1030 from 3 biological
874 replicates) (right panel). (B). Schematic of experimental design for time lapse experiment in
875 Fig. 3C-D. (C) Montage of cells expressing mt-mNeongreen stained with TMRE tracked over

876 time, imaged every 5 min for 40 min. TMRE was imaged only at t=0 of time lapse. (D) Scatter
877 plot with Mean form factor and number of mitochondria over time, plotted for cells starting
878 with MFF<2 at the beginning of time lapse. Each data point represents one cell with colour
879 corresponding to TMRE intensity normalized to cell area at t=0 min; n=61 for empty vector,
880 n=91 for mtDarT from 3 biological replicates. Statistical significance in A was calculated using
881 Mann-Whitney U test. (*** p<0.0001, ** p<0.005, * p< 0.05, n.s.- not significant, in all cases).

882 **Figure 4: Changes in mitochondrial morphology accompany loss of mtDNA but not**
883 **mitochondria.** (A). Montage of cells expressing Cox4::mCherry stained with SYBR Green I to
884 visualize mtDNA over time. (B). Percentage of cells over time without any mtDNA foci. Mean
885 ± SD from 3 biological replicates; n>100 in each biological replicate. (C). Cox4::mCherry and
886 Tom20::mCherry western blot with quantification from 3 biological replicates, normalized to
887 empty vector at t=0; Error bars: SD. Statistical significance in C was calculated using paired
888 Student's t-test.

889 **Figure 5: Exonuclease activity of the mtDNA polymerase, Mip1, is essential for mtDNA**
890 **maintenance.** (A) Schematic showing domain organization of Mip1, with amino acid
891 mutations for *mip1*$^{exo-}$ marked in red (D171A, E173A). (B) Percentage of cells over time
892 without any mtDNA foci (p^0) are plotted. Mean ± SD from three biological replicates; n>85 in
893 each biological replicate. (C) Representative images of *mip1*$^{exo-}$ cells expressing
894 Cox4::mCherry stained with SYBR Green I. Yellow arrows mark mitochondria devoid of
895 mtDNA. (D-E). Fraction of mtDNA in bud (number of mtDNA foci in bud/total number of
896 mtDNA foci in the mother-bud pair) is plotted against fraction cell area (area of the bud/total
897 area of the mother-bud pair) for both wild type and *mip1*$^{exo-}$ cells, after 4 hr (top panel) or 6
898 hr of induction (bottom panel). Black line represents mean and shaded region represents SD
899 (calculated after binning x-axis in bins of 0.05). R^2 values were obtained via Pearson's
900 Correlation; n>145 from 4 biological replicates for *mip1*$^{exo-}$ and 3 biological replicates for wild
901 type. Statistical significance in E was calculated using Fisher's F-test, applied on distributions
902 of residual values of all data points (distance from linear fit curve). Comparisons were made
903 to empty vector control of corresponding time point.

Figure 1

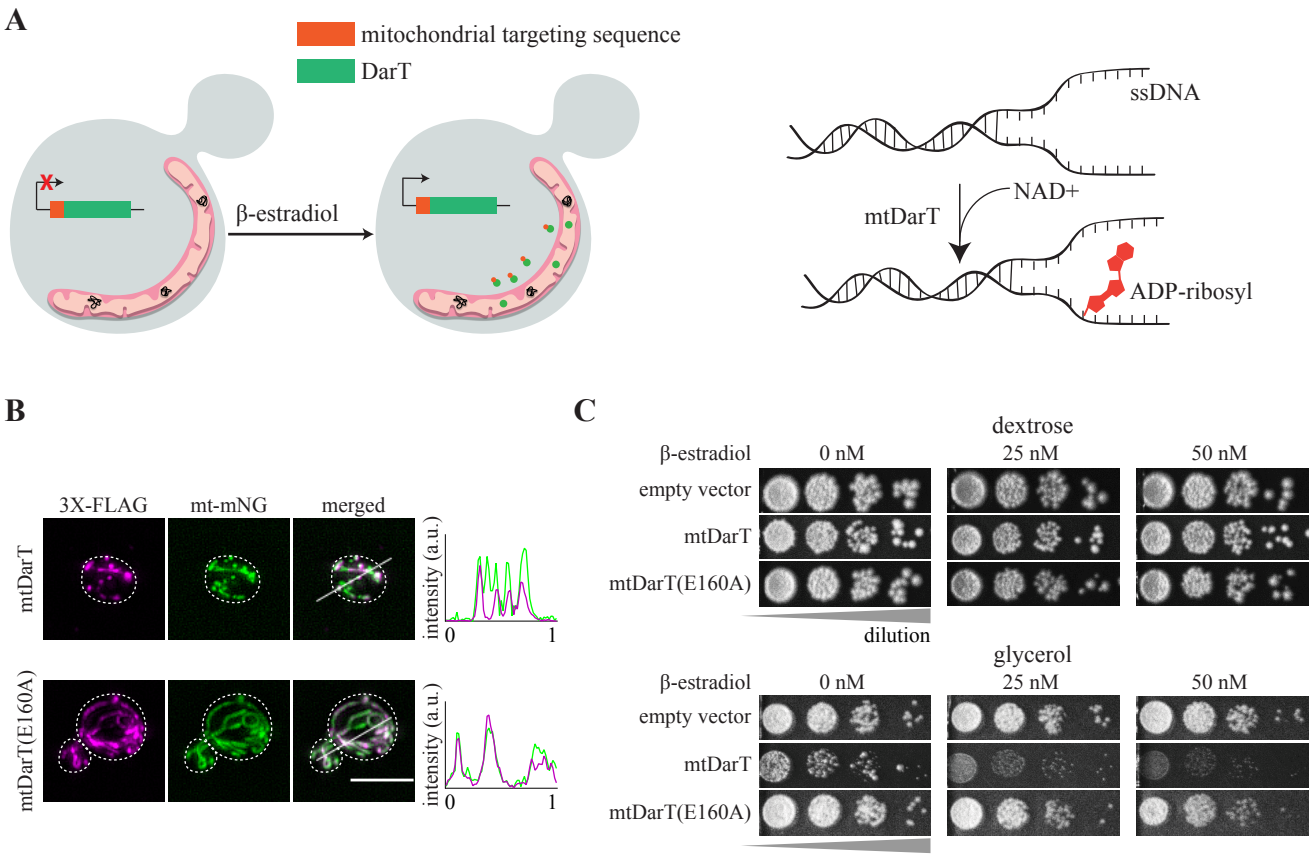
A
mitochondrial targeting sequence
DarT
β-estradiol
ssDNA
NAD+
mtDarT
ADP-ribosyl
B
3X-FLAG
mt-mNG
merged
mtDarT
mtDarT(E160A)
intensity (a.u.)
0
1
C
dextrose
glycerol
β-estradiol
0 nM
25 nM
50 nM
empty vector
mtDarT
mtDarT(E160A)
dilution

Figure 2

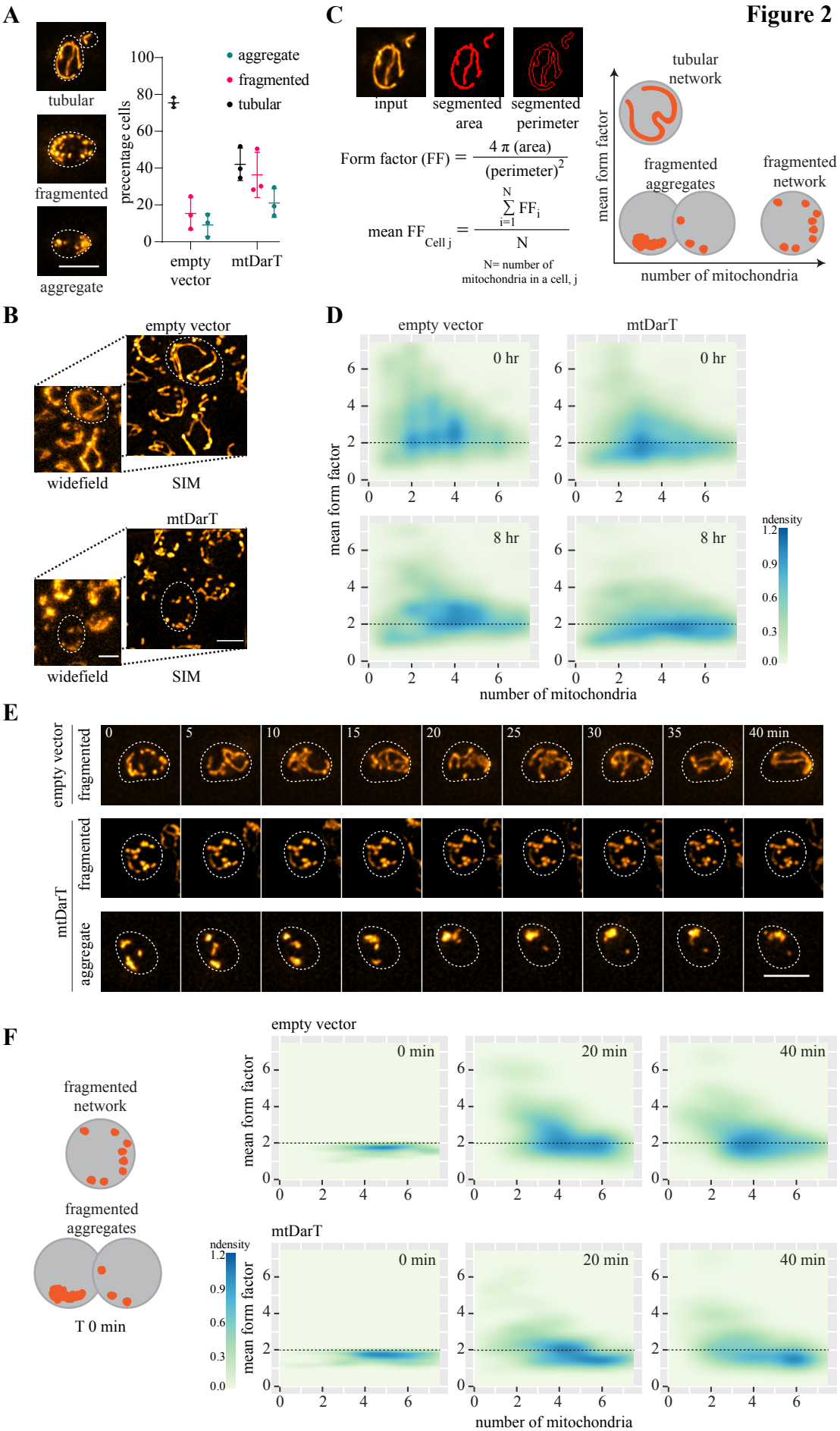
A
tubular
fragmented
aggregate
precentage cells
100
80
60
40
20
0
aggregate
fragmented
tubular
empty vector
mtDarT
B
empty vector
widefield
SIM
mtDarT
widefield
SIM
C
input
segmented area
segmented perimeter
Form factor (FF) = 4 π (area) / (perimeter)^2
mean FF Cell j = Σ FF_i (i=1 to N) / N
N= number of mitochondria in a cell, j
tubular network
fragmented aggregates
fragmented network
mean form factor
number of mitochondria
D
empty vector
mtDarT
0 hr
8 hr
mean form factor
ndensity
number of mitochondria
E
empty vector
fragmented
mtDarT
fragmented
aggregate
0
5
10
15
20
25
30
35
40 min
F
fragmented network
fragmented aggregates
T 0 min
empty vector
mtDarT
0 min
20 min
40 min
mean form factor
ndensity
number of mitochondria

Figure 3

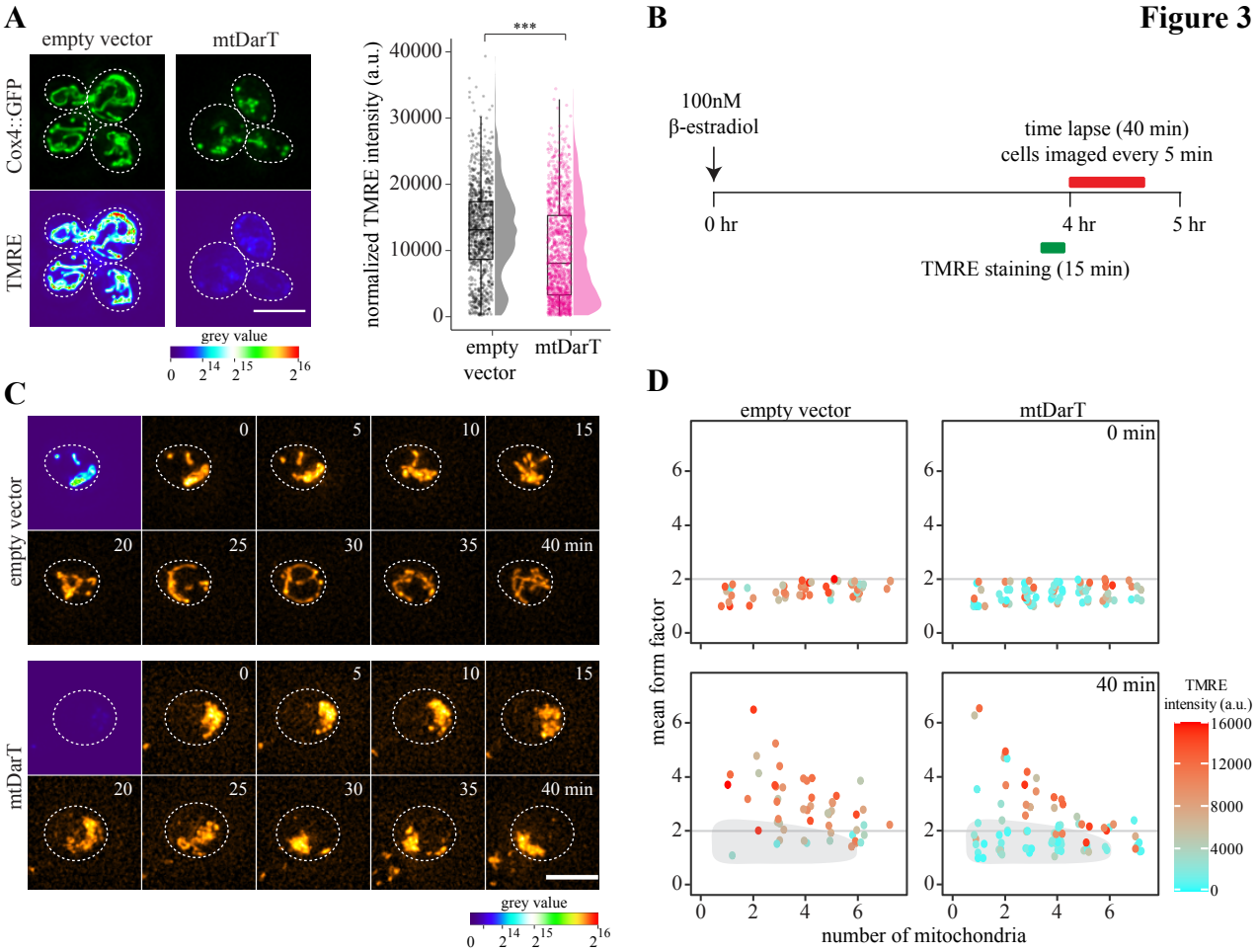
A
empty vector
mtDarT
Cox4::GFP
TMRE
grey value
0
2^14
2^15
2^16
normalized TMRE intensity (a.u.)
40000
30000
20000
10000
0
***
empty vector
mtDarT
B
100nM
β-estradiol
time lapse (40 min)
cells imaged every 5 min
0 hr
4 hr
5 hr
TMRE staining (15 min)
C
empty vector
mtDarT
0
5
10
15
20
25
30
35
40 min
grey value
D
empty vector
mtDarT
0 min
40 min
mean form factor
number of mitochondria
TMRE
intensity (a.u.)
16000
12000
8000
4000
0

Figure 4

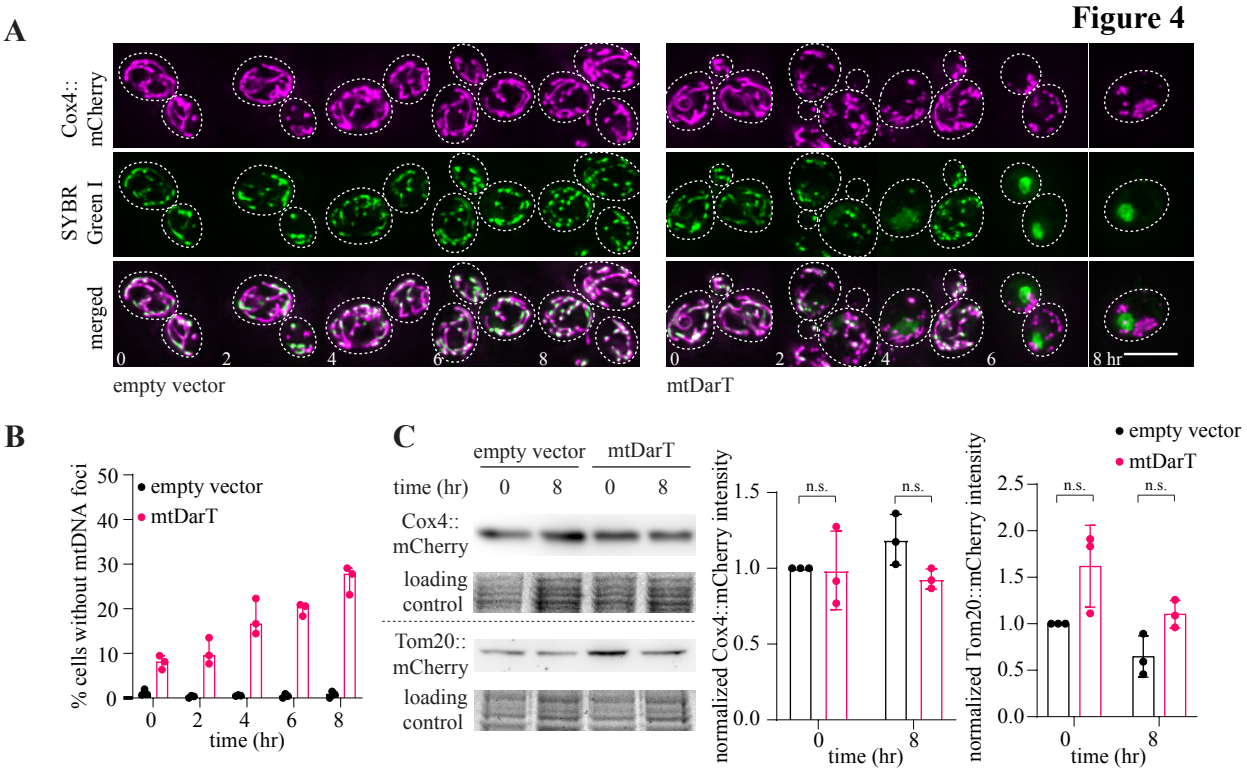
A
Cox4:: mCherry
SYBR Green I
merged
0
2
4
6
8
8 hr
empty vector
mtDarT
B
% cells without mtDNA foci
empty vector
mtDarT
time (hr)
C
empty vector
mtDarT
time (hr)
Cox4:: mCherry
loading control
Tom20:: mCherry
loading control
normalized Cox4::mCherry intensity
normalized Tom20::mCherry intensity
n.s.

Figure 5

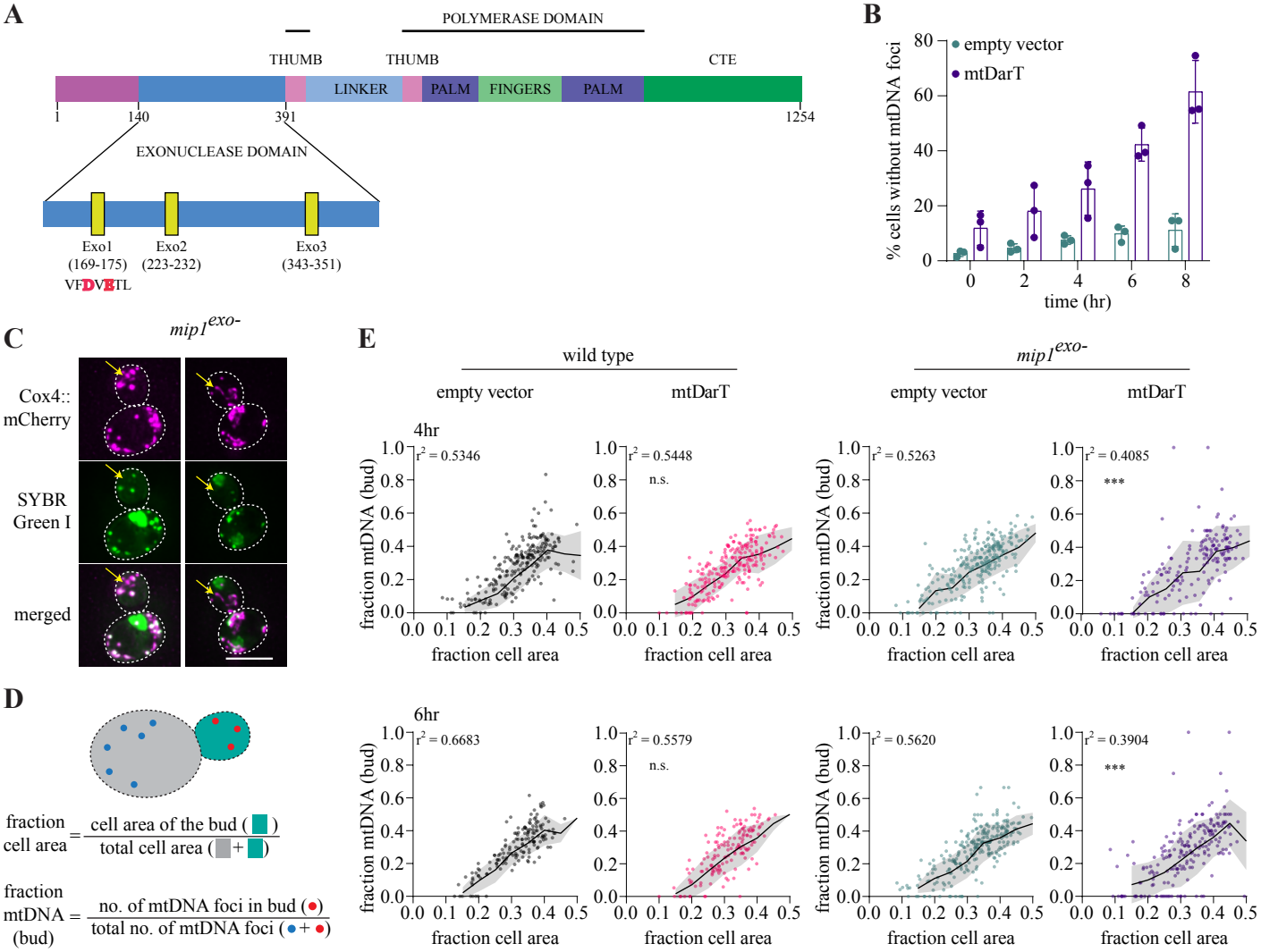
A
POLYMERASE DOMAIN
THUMB
THUMB
CTE
LINKER
PALM
FINGERS
PALM
1
140
391
1254
EXONUCLEASE DOMAIN
Exo1
(169-175)
Exo2
(223-232)
Exo3
(343-351)
VFDVETL
B
empty vector
mtDarT
% cells without mtDNA foci
time (hr)
C
mip1exo-
Cox4::
mCherry
SYBR
Green I
merged
D
fraction
cell area
cell area of the bud
total cell area
fraction
mtDNA
(bud)
no. of mtDNA foci in bud
total no. of mtDNA foci
E
wild type
mip1exo-
empty vector
mtDarT
empty vector
mtDarT
4hr
6hr
fraction mtDNA (bud)
fraction cell area
r2 = 0.5346
r2 = 0.5448
n.s.
r2 = 0.5263
r2 = 0.4085
***
r2 = 0.6683
r2 = 0.5579
n.s.
r2 = 0.5620
r2 = 0.3904
***

Supplementary information

Dynamic reorganization and selective segregation of mitochondria under DarT-mediated mtDNA damage

Nitish Dua, Akshaya Seshadri and Anjana Badrinarayanan*

National Centre for Biological Sciences - Tata Institute of Fundamental Research, Bellary Road, Bangalore 560065, Karnataka, India, Phone: 91 80 23666547

*Correspondence to: anjana@ncbs.res.in

Supplementary figure legends

Figure S1: System to induce mitochondria-specific DNA damage. (A) Schematic of β-estradiol inducible system. Transcription factor GAL4-HBD-VP16 is constitutively expressed under a pACT1 promoter, and is activated on binding of β-estradiol. The activated transcription factor binds to pGAL1 and initiates transcription of gene under this promoter. (B) Western blots of FLAG-tagged mtDarT/TE160A after 4 and 8 hr of induction with 100nM β-estradiol. (C) Representative cells expressing mt-mNeongreen and Cox4::mCherry (top panel), and cell expressing mt-mNeongreen stained with TMRE (bottom panel). (Scale bars-5µm, white dotted lines mark cell outlines, in all figures)

Figure S2: mtDNA damage impacts mitochondrial organization and dynamics. (A) Percentage of cells in each category in control (empty vector) or mtDarT cells at t=0hr (mean±SD from three biological replicates, n>150 in each replicate). (B) Schematic showing experimental design for time lapse experiments. (C) Montage of single cells expressing Cox4::mCherry tracked over time (mean form factor <2 at the beginning of the time lapse), imaged for 40 min after 4 hr of induction. (D) Density plots with mean form factor and number of mitochondria over time, plotted for cells starting with MFF>2 at the beginning of time lapse; n=362 for empty vector, n=347 for mtDarT from 3 biological replicates. (E) Dnm1::HA western blot with quantification from 3 biological replicates, normalized to empty vector at t=0; Error bars: SD. (F) Representative images of cells expressing Mdm34::mNeongreen and Cox4::mCherry after 8 hr of induction. Number of Mdm34 foci per cell are plotted from 3 biological replicates; n>680. Statistical significance in E was calculated using paired Student's t-test. (*** p<0.0001, ** p<0.005, * p< 0.05, n.s.- not significant, in all cases).

Figure S3: mtDNA damage impacts mitochondrial organization and dynamics. (A) Cell area plotted as violin plots for all the cells in Fig 2 and S2D at t=0 min. (B) Density plots with Mean form factor and number of mitochondria over time, plotted for cells in Fig 2F, classified based on presence or absence of buds.

Figure S4: mtDNA damage results in mitochondrial dysfunction. (A) Representative images of cells expressing Cox4::GFP stained with TMRE after treatment with FCCP (2 µM) for 20 min or Oligomycin (0.5 µg/ml) for 4 hr (left panel) (Cox4::GFP: green). Total TMRE intensity normalized to cell area is plotted; n>650 from 3 biological replicates for FCCP and Oligomycin and 2 biological replicates for empty vector (right panel). (B) Representative images of cells

expressing COX4::GFP stained with TMRE after 4 hr of induction with 100nM β-estradiol. Examples show cells from three different morphological categories for both empty vector and mtDarT (top panel). Total TMRE intensity normalized to cell area is plotted for cells with three mitochondrial morphologies, after 4 hr of induction (for empty vector, n=215 for tubular, n=35 for fragmented, n=30 aggregate; for mtDarT, n=258 for tubular, n=79 for fragmented, n=118 for aggregate). Statistical significance in A, B was calculated using Mann-Whitney U test.

Figure S5: Changes in mitochondrial morphology accompany loss of mtDNA but not mitochondria. (A) Number of mtDNA foci per cell after 8 hr of induction is plotted; n>930 from 3 biological replicates. (B) Representative cells imaged with Structured Illumination Microscopy with segmentation output after Mitograph analysis (left panel). Mitochondrial volume analysed using Mitograph, each data point represents one cell; n=12 for empty vector and n=24 for mtDarT. (C) Representative images of cells expressing GFP::Atg8 under the endogenous *ATG8* promoter treated with Rapamycin (20nM) for 4 hr and cells transformed with empty vector or mtDarT after 8 hs of induction with 100nM β-estradiol (left panel). Frequency distribution of number of GFP::Atg8 localization (right panel). (D) Vacuolar intensity of Idh1::GFP normalized to total cell intensity after 4 hr of induction with 100nM β-estradiol; n>830 from 2 biological replicates (left panel), with representative images of cells expressing Idh1::GFP and Vph1::mCherry (right panel). Statistical significance in A,B,D was calculated using Mann-Whitney U test.

Figure S6: Exonuclease activity of the mtDNA polymerase, Mip1, is essential for mtDNA maintenance. (A) Density plots with mean form factor and number of mitochondria over time for *mip1*$^{exo-}$ cells; n>710 in each plot, from 3 biological replicates. (B) Total TMRE intensity normalized to cell area for *mip1*$^{exo-}$ cells is plotted; n>1350 from 3 biological replicates. (C) Schematic summarizing key observations of this study. mtDNA damage triggers mitochondrial dysfunction and associated changes in mitochondrial organization. Exonuclease function of replicative polymerase, Mip1, is required to prevent rapid loss of mtDNA under damage. For details, see discussion. Statistical significance in B was calculated using Mann-Whitney U test.

Supplementary Table S1: Strains used in present study

Strain #	Strain name	Genotype	Source	Strain construction
NABC567	CEN.PK	*Mat a*	(van Dijken et al., 2000)	NA
NABC568	CEN.PK	*Mat α*	(van Dijken et al., 2000)	NA
NABC569	*COX4-mCherry*	CEN.PK a *COX4-mCherry-Hyg*	This study	mCherry-Hyg casette was amplified from NABC549 using oligos 14,15
NABC570	*COX4-GFP*	CEN.PK a *COX4-GFP-KanMX6*	This study	GFP-KanMX casette was amplified from NABC548 using oligos 14,15
NABC571	*DNM1-HA*	CEN.PK a *DNM1-HA-KanMX6*	This study	HA-KanMX casette was amplified from NABC550 using oligos 17,18
NABC572	*mip1Δ*	CEN.PK a *mip1Δ::KanMX6*	This study	KanMX caseete was amplified from NABC551 using oligos 26,27
NABC573	*mip1^{exo-}*	CEN.PK a *mip1Δ::mip1^{D171A,E173A}-Hyg*	This study	Oligos 22,23,24,25 used to amplify full length gene in two fragments, to do Gibson assembly with a Hyg casette amplified from NABC552.
NABC574	*TOM20-mCherry*	CEN.PK a *TOM20-mCherry-KanMX6*	SL lab stock	NA
NABC575	*MDM34-mNeongreen COX4-mCherry*	CEN.PK a *MDM34-mNeongreen-KanMX6 COX4-mCherry-Hyg*	This study	mNeongreen-KanMX cassette was amplified from NABC553 using oligos 20,21. The fragment was transformed in NABC569.
NABC576	*Su9-mNeongreen*	CEN.PK a *HO::P_{CYC1}-SU9-mNeongreen-T_{CYC1}-KanMX6*	This study	NABC556 plasmid was transformed in NABC567 to get HO-locus integration
NABC577	*IDH1-GFP VPH1-mCherry*	CEN.PK a *IDH1-GFP-KanMX6 VPH1-mCherry-Hyg*	This study	GFP-KanMX cassette was amplified from NABC548 (oligos 32,33), mCherry-Hyg cassette was amplified from NABC549 (oligos 34,35) and transformed into NABC567.

Supplementary Table S2: Plasmids used in present study

Plasmid #	Plasmid Name	Description	Source	Plasmid construction
NABC548	pFA6a-GFP-KanMX6	Used for C-terminal tagging with GFP and KanMX6 selection marker.	SL lab stock	NA
NABC549	pFA6a-mCherry-Hyg	Used for C-terminal tagging with mCherry and Hygromycin selection marker.	SL lab stock	NA
NABC550	pFA6a-HA-KanMX6	Used for C-terminal tagging with HA and KanMX6 selection marker.	SL lab stock	NA
NABC551	pFA6a-KO-KanMX6	Used for gene knockouts with KanMX6 selection marker.	SL lab stock	NA
NABC552	pFA6a-KO-Hyg	Used for gene knockouts with Hygromycin selection marker.	SL lab stock	NA
NABC553	pFA6a-mNeongreen-KanMX6	Used for C-terminal tagging with mNeongreen and KanMX6 selection marker. Codon optimized mNeongreen was cloned into the pFA6a plasmid background.	This Study	mNeongreen from plasmid NABC554 was cloned with tADH1 into pFA6a background between Pac1 and Bgl2 sites using Gibson cloning with oligos 28,29,30,31
NABC554	pMA-Su9-mNeongreen	Codon optimised Su9-mNeongreen sequence.	This Study	(Synthesized by ThermoFisher)
NABC555	p417-CYC	cen/ars plasmid, with weak cyc promoter for low expression of protein	SL lab stock	NA
NABC556	M4297 HO-pCYC1-Su9-mNEONgreen-tCYC1-KanMX6-HO	Used for integration of pCYC1-Su9-mNEONgreen-tCYC1-KanMX6 at HO locus. Plasmid contains overhangs for recombination at the HO locus.	This Study	pCYC1-Su9-mNeongreen-tCYC1 cloned at BamH1 site in NABC 565 using Gibosn cloning with oligos 1,2,3,4

NABC557	pGEV-3XFlag-NAT	*CEN/ARS* Plasmid containing constitutively expressed pGAL4-HBD-VP16 transcription factor under pACT1. Expression of genes cloned under pGAL1 promoter is induced on addition of β-estradiol.	SL lab stock	NA
NABC558	pACDH-DarG	DarG cloned under a Lac promoter (IPTG inducible).	This Study	DarG from NABC560 cloned into NABC566 at Nco1 site using Gibson cloning with oligos 5,6
NABC559	pBAD33-TaqDarT	DarT from *Thermus aquaticus* cloned in the pBAD33 plasmid. Expression is repressed in presence of glucose.	(Jankevicius et al., 2016)	NA
NABC560	pET28a-TaqDarG	DarG from *Thermus aquaticus* cloned in the pET28a plasmid. Expression is repressed in presence of glucose.	(Jankevicius et al., 2016)	NA
NABC561	pGEV-Su9-DarT-3XFlag-NAT	Su9-DarT was cloned at the PacI site downstream of pGAL1 and in frame with the linker-3XFlag sequence.	This Study	DarT from NABC559 cloned with Su9 in NABC557 at PacI site using Gibson cloning with oligos 7,10,11,12
NABC562	pGEV-Su9-DarT(E160A)-3XFlag-NAT	Su9-DarT(E160A) was cloned at the PacI site downstream of pGAL1 and in frame with the linker-3XFlag sequence.	This Study	DarT from NABC559 cloned with Su9 in NABC557 at PacI site using Gibson cloning with oligos 7,10,11,12 and oligos 8,9 to introduce mutations

NABC563	GFP-ATG8(416)	N-terminally GFP tagged ATG8 expressed under the control of endogeneous promoter in a pRS416 vector	Addgene (Plasmid #49425) (Guan et al., 2001)	NA
NABC564	p417-GFP-ATG8(416)	GFP-Atg8(416) along with Atg8 promoter cloned between SacI and EcoRI sites	This Study	GFP-Atg8 with endogeneous Atg8 promoter was cloned from NABC563 into NABC555 by restriction digestion and ligation using restriction sites for SacI and EcoRI
NABC565	M4297HO Kan	HO-locus integration plasmid with KanMX selection marker	SL lab stock	NA
NABC566	pACDH	Plasmid with a lac promoter and a p15a ori	SL lab stock	NA

Supplementary Table S3: Oligos used in present study

Oligo #	Oligo sequence (5'-3')
Oligo 1	cgcaaacacaaatacacacactaatctagaATGGCTTCTACTAGAGTTTTGGCTTCTAGA TTGGCTTCTCA
Oligo 2	ctgcagcccgggggatccactagttctagaTCAAGAATTAGAAGAAGCAGAACCTGAACC TGCAGCAGA
Oligo 3	TTAAAATGGCGTCGTACGCTGCAGGTCGACGGATCCcatttggcgagcgttggttggtggatcaag
Oligo 4	AACAGATCTGGCGCGCCTTAATTAACCCGGGGATCCgcaaattaaagccttcgagcg tcccaaaaccttctc
Oligo 5	GTTTAACTTTAAGAAGGAGATATACCATGGATGCTGCGTTTCGTTCGCGGTAAC
Oligo 6	TTTGCTGTCCACCAGTCATGCTAGCCATGGTTACGCTTCTTGAGCAACATT TGCCGGC
Oligo 7	GATACTCAAAGATATCCCCGGGTTAATTAAATGGCTTCTACTAGAGTTTT GGCTTCTAG
Oligo 8	CTTTGACCAGAAATGCGGCCTGTTTC
Oligo 9	GAAACAGGCCGCATTTCTGGTCAAAG
Oligo 10	GTCATCGTCATCTTTATAATCGTTAATTAAGAACGTGGCTTCACAGGACGCACTGC
Oligo 11	AACCGGATAAGCCAGACCCTGTTGCGGCAT AGAAGAGTAGGCCCTTTTT TGAAAAGC
Oligo 12	ATGCCGCAACAGGGTCTGGCTTATCC
Oligo 13	GAAAACTGCCCAAAACTTAG
Oligo 14	ACTAAACCCTGTTGGTGTTCCAAATGATGACCACCATCACcggatccccgggttaattaa
Oligo 15	GTAAAAGAGAAACAGAAGGGCAACTTGAATGATAAGATTAgaattcgagctcgtttaaac
Oligo 16	CGGTGATGGAAATATTGAAG
Oligo 17	AGTTTATAAAAAGGCTGCAACCCTTATTAGTAATATTCTGcggatccccgggttaattaa
Oligo 18	TGTTGAAGTAAGATCAAAAATGAGATGAATTATGCAATTAgaattcgagctcgtttaaac
Oligo 19	GATTCAGTCTCGACTTTTCG
Oligo 20	CTGGAAATGGGGCATGGAGGATAGCCCCCCACCATATCATcggatccccgggttaattaa
Oligo 21	TATTTGTGTAGTTATGTACTTAGATATGTAACTTAATTTAgaattcgagctcgtttaaac
Oligo 22	TATGTAGTTGTTGAGCAACGAGGGACAAGTATGACGAAATTGATGGTTAG ATCTGAATGCATGCTG
Oligo 23	CTGGTGGTGTTTGCTGTAGCAACACTCTATAAC
Oligo 24	CGTTATAGAGTGTTGCTACAGCAAACACCACCAG
Oligo 25	CTAGTACTCTCTAGAAATAGTAATGTCCCTTTCCAG
Oligo 26	GGGATTATATGTAGTTGTTGAGCAACGAGGGACAAGTATGcggatccccgggttaattaa
Oligo 27	ATATAAATACAAATGCGAAAGCTAATGCAGATTTTGCCTAgaattcgagctcgtttaaac
Oligo 28	TGCAGGTCGAcggatccccgggttaattaaCATGGCTTCTTTGCCAGCTAC
Oligo 29	aataaaaatcataaatcataagaaattcgcTCAAGAATTAGAAGAAGCAGAACCTGAA
Oligo 30	gcgaatttcttatgatttatgattt
Oligo 31	cggcggggacgaggcaagctaaacagatct
Oligo 32	TGACTTCACGAATGAAATCATCAACAAATTATCTACCATGcggatccccgggttaattaa
Oligo 33	TTAAGTTGCAGAACAAAAAAAAGGGGAATTGTTTTCATTAgaattcgagctcgtttaaac
Oligo 34	GGAAGTCGCTGTTGCTAGTGCAAGCTCTTCCGCTTCAAGCcggatccccgggttaattaa
Oligo 35	ACTTAAATGTTTCGCTTTTTTTAAAAGTCCTCAAAATTTAgaattcgagctcgtttaaac

Supplementary references

Guan, J., Stromhaug, P. E., George, M. D., Habibzadegah-Tari, P., Bevan, A., Dunn, W. A., & Klionsky, D. J. (2001). Cvt18/Gsa12 is required for cytoplasm-to-vacuole transport, pexophagy, and autophagy in Saccharomyces cerevisiae and Pichia pastoris. *Molecular Biology of the Cell*, *12*(12), 3821–3838. https://doi.org/10.1091/mbc.12.12.3821

Jankevicius, G., Ariza, A., Ahel, M., & Ahel, I. (2016). The Toxin-Antitoxin System DarTG Catalyzes Reversible ADP-Ribosylation of DNA. *Molecular Cell*, *64*(6), 1109–1116. https://doi.org/10.1016/j.molcel.2016.11.014

van Dijken, J. P., Bauer, J., Brambilla, L., Duboc, P., Francois, J. M., Gancedo, C., Giuseppin, M. L. F., Heijnen, J. J., Hoare, M., Lange, H. C., Madden, E. A., Niederberger, P., Nielsen, J., Parrou, J. L., Petit, T., Porro, D., Reuss, M., van Riel, N., Rizzi, M., … Pronk, J. T. (2000). An interlaboratory comparison of physiological and genetic properties of four Saccharomyces cerevisiae strains. *Enzyme and Microbial Technology*, *26*(9), 706–714. https://doi.org/10.1016/S0141-0229(00)00162-9

Figure S1

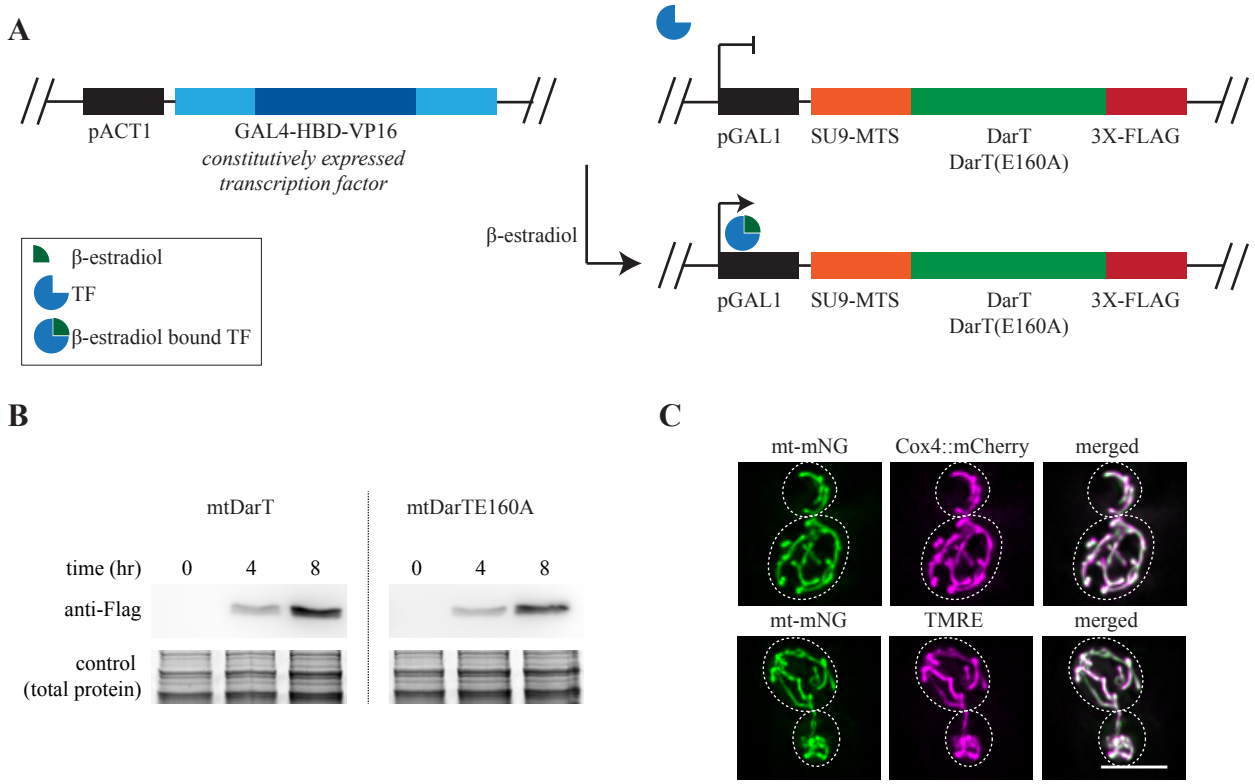
A
pACT1
GAL4-HBD-VP16
constitutively expressed
transcription factor
β-estradiol
TF
β-estradiol bound TF
β-estradiol
pGAL1
SU9-MTS
DarT
DarT(E160A)
3X-FLAG
pGAL1
SU9-MTS
DarT
DarT(E160A)
3X-FLAG
B
mtDarT
mtDarTE160A
time (hr)
0
4
8
0
4
8
anti-Flag
control
(total protein)
C
mt-mNG
Cox4::mCherry
merged
mt-mNG
TMRE
merged

Figure S2

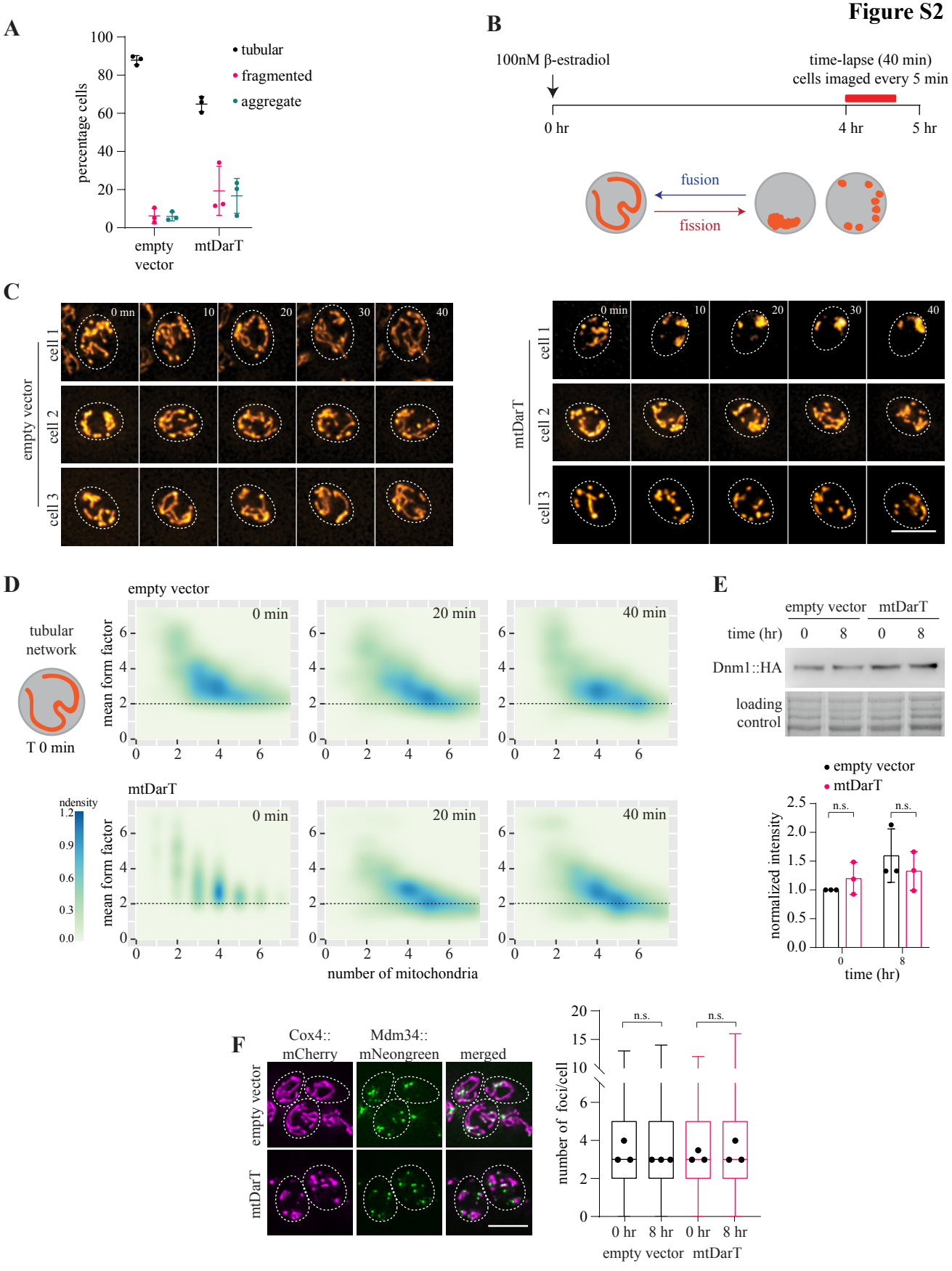
A
percentage cells
tubular
fragmented
aggregate
empty vector
mtDarT
B
100nM β-estradiol
time-lapse (40 min)
cells imaged every 5 min
0 hr
4 hr
5 hr
fusion
fission
C
empty vector
cell 1
cell 2
cell 3
0 mn
10
20
30
40
mtDarT
0 min
D
empty vector
tubular network
T 0 min
mean form factor
0 min
20 min
40 min
mtDarT
ndensity
number of mitochondria
E
empty vector
mtDarT
time (hr)
Dnm1::HA
loading control
normalized intensity
n.s.
time (hr)
F
Cox4:: mCherry
Mdm34:: mNeongreen
merged
empty vector
mtDarT
number of foci/cell
0 hr
8 hr

Figure S3

A

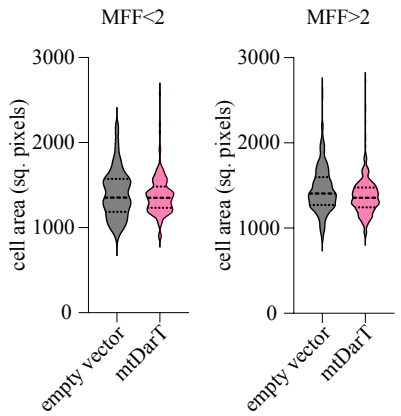
MFF<2
MFF>2
cell area (sq. pixels)
3000
2000
1000
0
empty vector
mtDarT

B

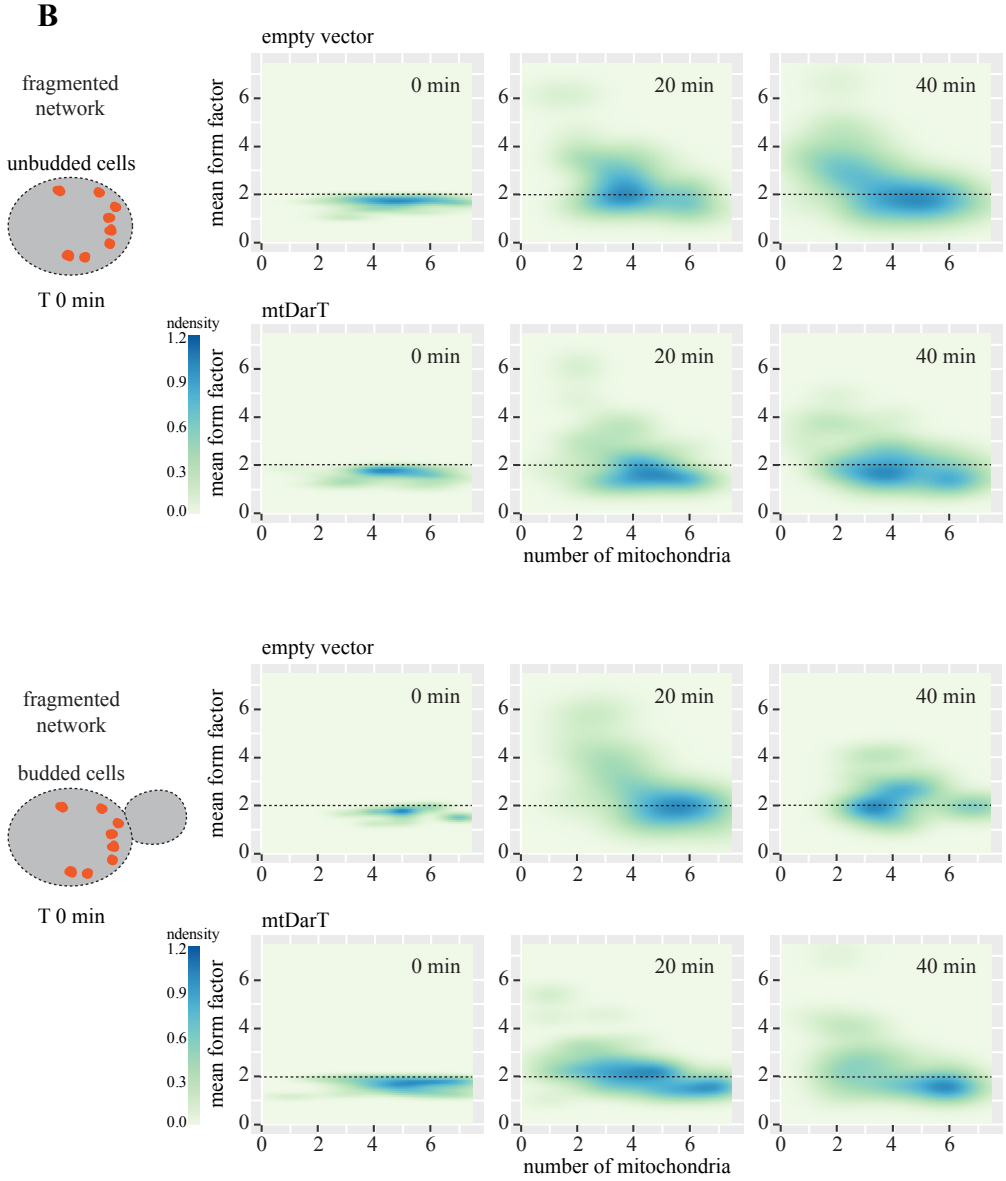
empty vector
fragmented network
unbudded cells
T 0 min
mtDarT
ndensity
1.2
0.9
0.6
0.3
0.0
mean form factor
0 min
20 min
40 min
number of mitochondria
fragmented network
budded cells

Figure S4

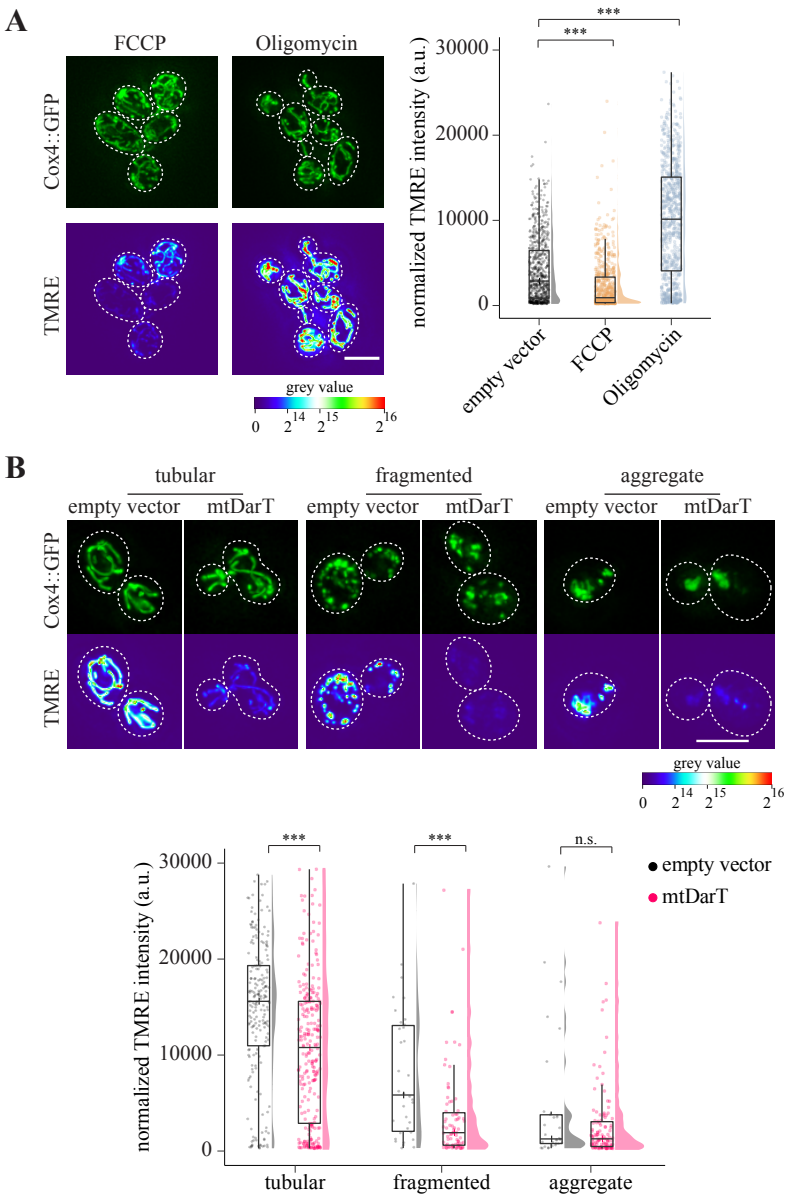
A
FCCP
Oligomycin
Cox4::GFP
TMRE
grey value
0
2^14
2^15
2^16
normalized TMRE intensity (a.u.)
30000
20000
10000
0
***
***
empty vector
FCCP
Oligomycin
B
tubular
fragmented
aggregate
empty vector
mtDarT
empty vector
mtDarT
empty vector
mtDarT
Cox4::GFP
TMRE
grey value
0
2^14
2^15
2^16
normalized TMRE intensity (a.u.)
30000
20000
10000
0
***
***
n.s.
empty vector
mtDarT
tubular
fragmented
aggregate

Figure S5

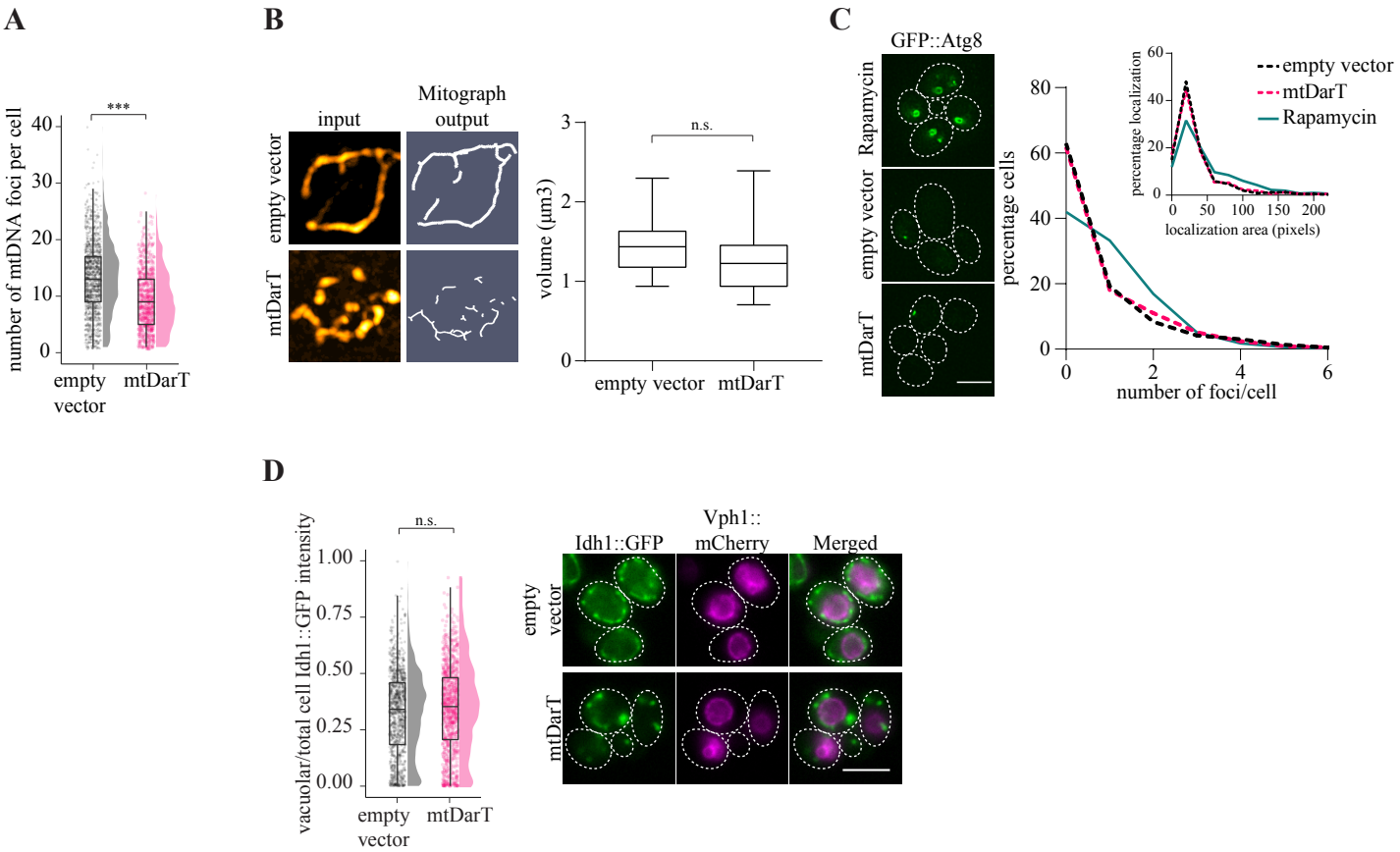
A
number of mtDNA foci per cell
***
empty vector
mtDarT
B
input
Mitograph output
empty vector
mtDarT
volume (µm3)
n.s.
empty vector
mtDarT
C
GFP::Atg8
Rapamycin
empty vector
mtDarT
percentage cells
number of foci/cell
percentage localization
localization area (pixels)
empty vector
mtDarT
Rapamycin
D
vacuolar/total cell Idh1::GFP intensity
n.s.
empty vector
mtDarT
Idh1::GFP
Vph1:: mCherry
Merged
empty vector
mtDarT

Figure S6

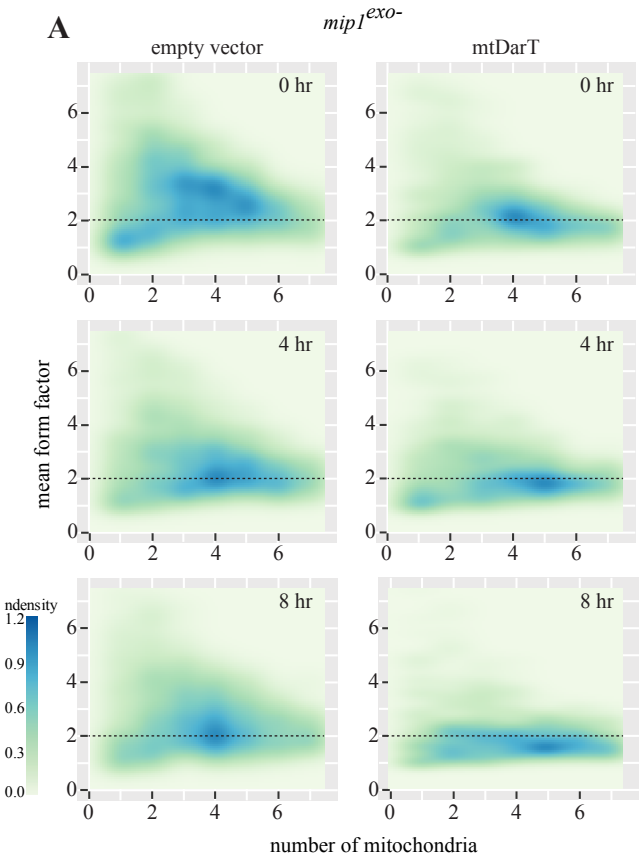
A
mip1exo-
empty vector
mtDarT
0 hr
4 hr
8 hr
mean form factor
ndensity
1.2
0.9
0.6
0.3
0.0
number of mitochondria

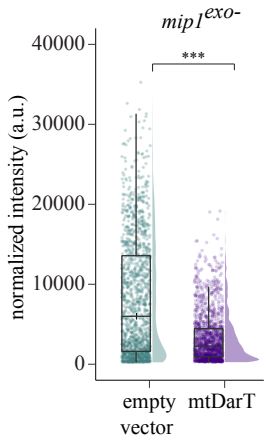
B
mip1exo-
***
normalized intensity (a.u.)
40000
30000
20000
10000
0
empty vector
mtDarT

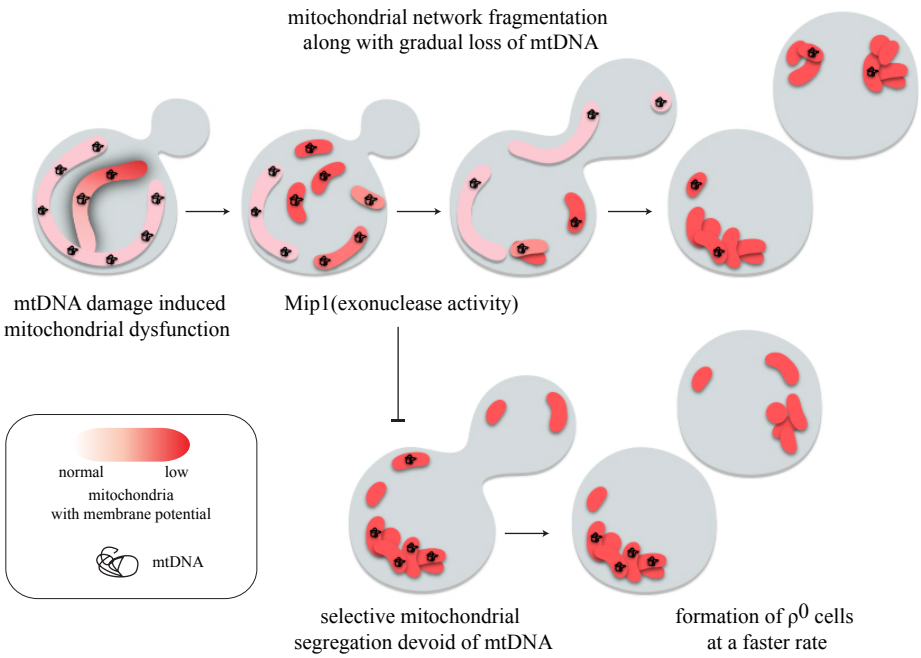
C
mitochondrial network fragmentation
along with gradual loss of mtDNA
mtDNA damage induced
mitochondrial dysfunction
Mip1(exonuclease activity)
normal
low
mitochondria
with membrane potential
mtDNA
selective mitochondrial
segregation devoid of mtDNA
formation of ρ0 cells
at a faster rate